polymers

MDPI

Article

Single and Double-Stranded 1D-Coordination Polymers with 4′-(4-Alkyloxyphenyl)-3,2′:6′,3″-terpyridines and $\{Cu_2(\mu\text{-}OAc)_4\}$ or $\{Cu_4(\mu_3\text{-}OH)_2(\mu\text{-}OAc)_2(\mu_3\text{-}OAc)_2(AcO\text{-}\kappa O)_2\}$ Motifs

Dalila Rocco [1], Giacomo Manfroni [1], Alessandro Prescimone [1], Y. Maximilian Klein [2], Dariusz J. Gawryluk [2], Edwin C. Constable [1] and Catherine E. Housecroft [1,*]

[1] Department of Chemistry, University of Basel, BPR 1096, Mattenstrasse 24a, CH-4058 Basel, Switzerland; dalila.rocco@unibas.ch (D.R.); giacomo.manfroni@unibas.ch (G.M.); alessandro.prescimone@unibas.ch (A.P.); edwin.constable@unibas.ch (E.C.C.)

[2] Laboratory for Multiscale Materials Experiments, Paul Scherrer Institut, CH-5232 Villigen PSI, Switzerland; maximilian.klein@psi.ch (Y.M.K.); dariusz.gawryluk@psi.ch (D.J.G.)

* Correspondence: catherine.housecroft@unibas.ch; Tel.: +41-61-207-1008

Received: 17 December 2019; Accepted: 29 January 2020; Published: 4 February 2020

Abstract: Five coordination polymers formed from combinations of copper(II) acetate and 4′-(4-alkyloxyphenyl)-3,2′:6′,3″-terpyridines with methoxy (**1**), *n*-butoxy (**2**), *n*-pentyloxy (**3**) and *n*-heptyloxy (**4**) substituents are reported. Reaction of **1** with $Cu(OAc)_2{\cdot}H_2O$ leads to the 1D-polymer $[Cu_2(\mu\text{-}OAc)_4(\mathbf{1})]_n$ in which $\{Cu_2(\mu\text{-}OAc)_4\}$ paddle-wheel units are connected by ligands **1**, or $[\{Cu_4(\mu_3\text{-}OH)_2(\mu\text{-}OAc)_2(\mu_3\text{-}OAc)_2(AcO\text{-}\kappa O)_2(\mathbf{1})_2\}{\cdot}2MeOH]_n$ in which centrosymmetric tetranuclear clusters link pairs of ligands **1** to give a double-stranded 1D-polymer. Layering solutions of $Cu(OAc)_2{\cdot}H_2O$ (in MeOH) over **2**, **3** or **4** (in $CHCl_3$) leads to the assembly of the 1D-polymers $[2\{Cu_2(\mu\text{-}OAc)_4(\mathbf{2})\}{\cdot}1.25MeOH]_n$, $[Cu_2(\mu\text{-}OAc)_4(\mathbf{3})]_n$ and $[\{Cu_2(\mu\text{-}OAc)_4(\mathbf{4})\}{\cdot}0.2CHCl_3]_n$. In all compounds, the 3,2′:6′,3″-tpy unit coordinates only through the outer pyridine rings, but the conformation of the 3,2′:6′,3″-tpy responds to changes in the length of the alkyloxy tails leading to changes in the conformation of the polymer backbone and in the packing of the chains in the crystal lattice in the chains featuring $\{Cu_2(\mu\text{-}OAc)_4\}$ paddle-wheel linkers.

Keywords: 3,2′:6′,3″-terpyridine; 1D-coordination polymer; copper(II) acetate; multinuclear cluster

1. Introduction

The directional assembly of coordination polymers and networks depends upon the compatibility of directing-nodes and linkers [1]. Directional metal nodes are key to the rational design of 2- and 3-dimensional inorganic materials and is at the heart of 'reticular chemistry' in which well-defined molecular units, so-called secondary building units (SBUs), are used to direct extended frameworks in a pre-determined and controlled fashion [2,3]. One of the simplest SBUs is the $M_2(\mu\text{-}O_2CR)_4$ paddle-wheel motif in which the axial sites of the dinuclear core provide linear directionality (Scheme 1) [4,5]. The manner in which the $M_2(\mu\text{-}O_2CR)_4$ units are connected in a coordination network depends upon the nature of the linkers, and also whether the R group in the bridging carboxylate is coordinatively innocent or not. In a simple case, where R is non-coordinating, and the organic linker is a rigid rod, such as 4,4′-bipyridine (4,4′-bpy), a topologically and structurally linear 1D-chain is assembled, as for example in $[Mo_2(\mu\text{-}O_2C^tBu)_4(4,4'\text{-bpy})]_n$ [6]. 3D-frameworks can be achieved by retaining a rigid linker, such as 4,4′-bpy, but introducing paddle-wheel units which incorporate multifunctional

carboxylate ligands as exemplified by Zou and coworkers [7]. The use of organic dicarboxylates for connected paddle-wheel motifs in combination with rigid bidentate linkers is an established strategy for MOF design [8,9]. Once we move away from rigid-rod linkers, assembly algorithms become less predictable [10].

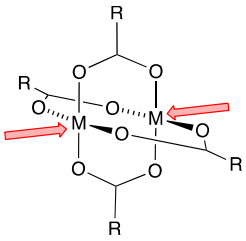

Scheme 1. Representation of an $\{M_2(\mu\text{-}O_2CR)_4\}$ paddle-wheel secondary building unit (SBU) with available coordination sites.

We are particularly interested in the use of two isomers of terpyridine, 3,2′:6′,3″-terpyridine (3,2′:6′,3″-tpy, IUPAC PIN $1^3,2^2:2^6,3^3$-terpyridine) and 4,2′:6′,4″-terpyridine (4,2′:6′,4″-tpy, PIN $1^4,2^2:2^6,3^4$-terpyridine) as both organic linkers and nodes in network assemblies [11,12]. Scheme 2 illustrates that in contrast to the archetypal 2,2′:6′,2″-terpyridine (tpy, PIN $1^2,2^2:2^6,3^2$-terpyridine), 3,2′:6′,3″-tpy and 4,2′:6′,4″-tpy do not bind metal ions by chelation, neither is the central nitrogen atom in 3,2′:6′,3″-tpy and 4,2′:6′,4″-tpy involved in metal coordination [13,14]. Combinations of 4,2′:6′,4″-tpy or its 4′-substituted derivatives with $\{M_2(\mu\text{-}O_2CR)_4\}$ (M = Cu, Zn; R is non-coordinating) units leads to 1D-coordination polymers which are topologically linear, but possess a zigzag structure by virtue of the 120° angle subtended by the outer donors at the central pyridine ring (Scheme 2) [15–20]. Although paddle-wheel SBUs are typical, there is also the possibility of assembling higher nuclearity motifs. For example, the reaction of $Zn(OAc)_2{\cdot}2H_2O$ with 4′-(pentafluorobiphenyl-4-yl)-4,2′:6′,4″-tpy yields crystals of the expected zigzag 1D-coordination polymer $[Zn_2(\mu\text{-}OAc)_4(4'\text{-}(2',3',4',5',6'\text{-pentafluoro-[1,1′-biphenyl]-4-yl})\text{-}4,2':6',4''\text{-tpy})]_n$ in addition to crystals of $[\{Zn_5(OAc)_{10}(4'\text{-}(2',3',4',5',6'\text{-pentafluoro-[1,1′-biphenyl]-4-yl})\text{-}4,2':6',4''\text{-tpy})\}{\cdot}11H_2O]_n$ in the same crystallization tube [17]. The latter comprises quadruple-stranded polymer chains supported by $\{Zn_5(OAc)_{10}\}$ units. Multiple-stranded 1D-coordination polymers have also been observed when cadmium(II) acetate or manganese(II) acetate react with some 4′-substituted 4,2′:6′,4″-tpy ligands, again as a result of the assembly of non-paddle-wheel SBUs [19,21]. The presence of co-ligands often complicates the picture as in the assembly of $[\{Zn_6(4\text{-pytpy})_3(mal)_4\}{\cdot}5H_2O]_n$ where 4-pytpy = 4′-(4-pyridyl)-4,2′:6′,4″-terpyridine and H_2mal = malic acid (2-hydroxybutanedioic acid) [22].

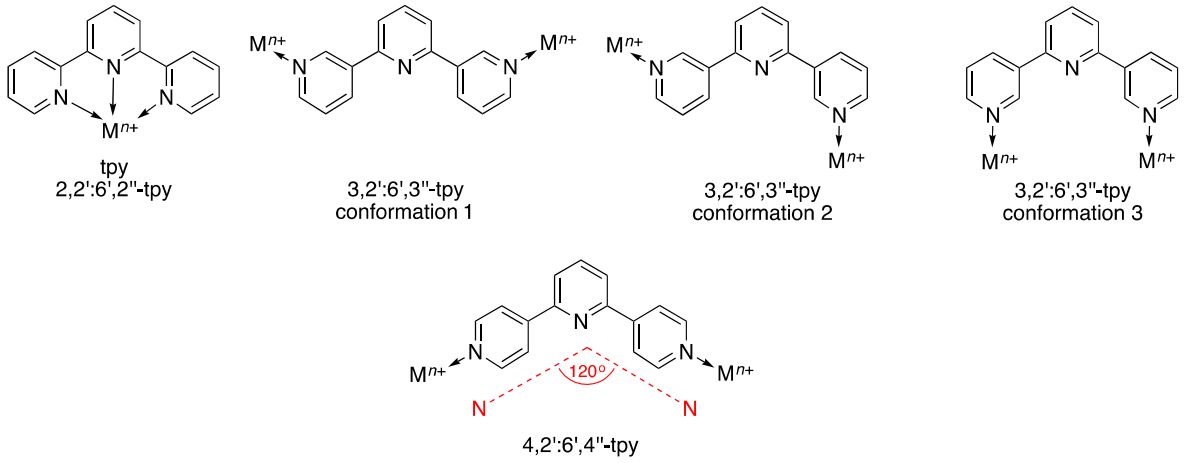

Scheme 2. Chelating metal-binding mode of tpy (monotopic ligand) versus ditopic metal-binding modes of 3,2′:6′,3″-tpy and 4,2′:6′,4″-tpy.

In a systematic investigation of reactions of zinc(II) acetate with the 4′-(4-alkyloxyphenyl)-4,2′:6′,4″-tpy ligands shown in Scheme 3, we observed the formation of zigzag 1D-coordination polymers $[Zn_2(\mu\text{-}OAc)_4(4'\text{-}(4\text{-alkyloxyphenyl})\text{-}4,2':6',4''\text{-tpy})]_n$ for short chains (R = Me, Et or ^{n}Pr in Scheme 3), but for *n*-octyloxy, *n*-nonyloxy and *n*-decyloxy substituents, discrete $[Zn_2(\mu\text{-}OAc)_4(4'\text{-}(4\text{-alkyloxyphenyl})\text{-}4,2':6',4''\text{-tpy})_2]$ coordination complexes were formed. For intermediate chain-lengths, the assembly pathways appear to compete with one another, and the packing of 1D-coordination polymers responds to the longer alkyloxy substituents with changes in the π-stacking motifs and by the incorporation of solvent or AcOH molecules into the crystal lattice [20]. A switch from 4,2′:6′,4″-tpy to 3,2′:6′,3″-tpy brings with it greater conformational flexibility. Both ligands possess rotational freedom about the inter-annular C–C bonds. Whereas this rotation has no effect on the vectorial arrangement of the outer-ring nitrogen lone pairs in 4,2′:6′,4″-tpy, it does cause conformational changes in 3,2′:6′,3″-tpy. The metal-binding arrangements shown in the middle diagrams in Scheme 2, are two possible vectorial arrangements of the nitrogen lone pairs. We were, therefore, interested in exploring how the structures of coordination assemblies formed from combinations of $\{M_2(\mu\text{-}OAc)_4\}$ paddle-wheel units with 4′-(4-alkyloxyphenyl)-3,2′:6′,3″-tpy ligands were influenced by changes in the length of the alkyloxy tails. Zhang and coworkers have reported that copper(II) acetate reacts with 4′-(4-*n*-hexyloxyphenyl)-3,2′:6′,3″-tpy to give a 1D-coordination polymer [23]. Coordination polymers and networks featuring ditopic 3,2′:6′,3″-tpy linkers are relatively scarce [24–28], although related ligands incorporating additional donors such as carboxylates and sulfonates have received some attention, as illustrated by examples in references [29–31]. Tetratopic ligands containing two 3,2′:6′,3″-motifs [11,32] have also been described. Herein we report the reactions of copper(II) acetate with ligands **1**–**4** (Scheme 4).

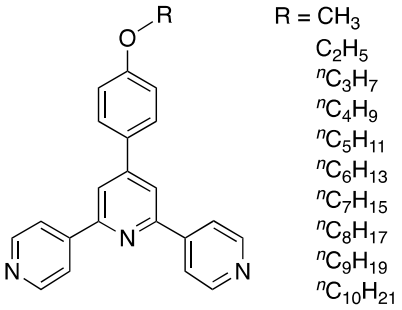

Scheme 3. 4′-(4-Alkyloxyphenyl)-4,2′:6′,4″-tpy ligands employed in a previous investigation [20].

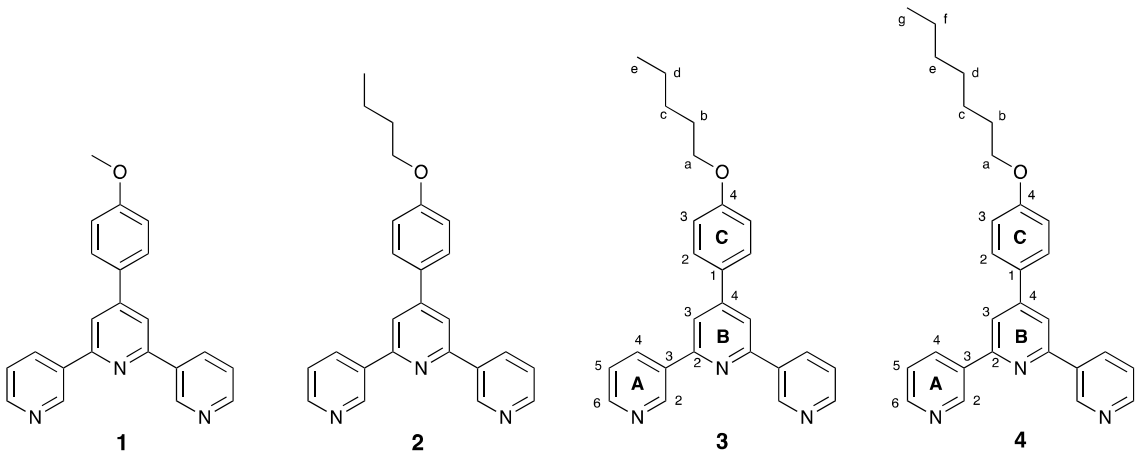

Scheme 4. Structures of ligands **1**–**4**, with atom numbering for NMR spectroscopic assignments of **3** and **4**.

2. Materials and Methods

2.1. General

^{1}H and ^{13}C{^{1}H} NMR spectra were recorded on a Bruker Avance III-500 spectrometer (Bruker BioSpin AG, Fällanden, Switzerland) at 298 K. The ^{1}H and ^{13}C NMR chemical shifts were referenced with respect to residual solvent peaks (δ TMS = 0). Electrospray ionization (ESI) mass spectra were recorded using a Shimadzu LCMS-2020 instrument (Shimadzu Schweiz GmbH, Reinach, Switzerland) and samples were introduced as MeCN solutions with a drop of formic acid added. A PerkinElmer UATR Two (Perkin Elmer, Schwerzenbach, Switzerland) and Cary-5000 (Agilent Technologies Inc., Santa Clara, CA, USA) or Shimadzu UV2600 (Shimadzu Schweiz GmbH, Reinach, Switzerland) spectrophotometer were used to record FT-infrared (IR) and absorption spectra, respectively.

Compounds **1** [33] and **2** [34] were prepared as previously reported. $Cu(OAc)_2{\cdot}H_2O$ was purchased from Fluka (Fluka Chemie GmbH, Buchs, Switzerland) 4-pentyloxybenzaldehyde from Combi-Blocks (Chemie Brunschwig AG, Basel, Switzerland), 4-heptyloxybenzaldehyde from Alfa Aesar (Thermo Fisher GmbH, Kandel, Germany) and were used as received.

2.2. Compound **3**

4-Pentyloxybenzaldehyde (1.92 g, 1.88 mL, 10 mmol) was dissolved in EtOH (50 mL), and then 3-acetylpyridine (2.42 g, 2.20, ml 20 mmol) and crushed KOH (1.12 g, 20 mmol) were added to the solution. The color changed to orange. Aqueous NH_3 (32%, 38.5 mL) was slowly added to the reaction mixture, and this was stirred at room temperature (ca. 22 °C) overnight. The precipitate that formed was collected by filtration, washed with EtOH (3 × 10 mL), recrystallized from EtOH and dried *in vacuo*. Compound **3** was isolated as a white powder (0.93 g, 2.23 mmol, 23.5%). M.p. = 116 °C. ^{1}H NMR (500 MHz, $CDCl_3$): δ/ppm = 9.37 (dd, J = 2.3, 0.9 Hz, 2H, H^{A2}), 8.70 (dd, J = 4.8, 1.7 Hz, 2H, H^{A6}), 8.51 (dt, J = 7.9, 2.3 Hz, 2H, H^{A4}), 7.93 (s, 2H, H^{B3}), 7.71 (m, 2H, H^{C2}), 7.46 (ddd, J = 7.9, 4.8, 0.9 Hz, 2H, H^{A5}), 7.07 (m, 2H, H^{C3}), 4.05 (t, J = 6.6 Hz, 2H, H^{a}), 1.84 (m, 2H, H^{b}), 1.49 (m, 2H, H^{c}), 1.42 (m, 2H, H^{d}), 0.96 (t, J = 7.2 Hz 3H, H^{e}). ^{13}C{^{1}H} NMR (500 MHz, $CDCl_3$): δ/ppm = 160.6 (C^{C4}), 155.4 (C^{A3}), 150.6 (C^{B4}), 150.2 (C^{A6}), 148.5 (C^{A2}), 135.0 (C^{A4}), 134.7 (C^{B2}), 130.3 (C^{C1}), 128.5 (C^{C2}), 123.8 (C^{A5}), 117.3 (C^{B3}), 115.4 (C^{C3}), 68.4 (C^{a}), 29.1 (C^{b}), 28.4 (C^{c}), 22.6 (C^{d}), 14.2 (C^{e}). UV-VIS (CH_3CN, 2.5×10^{-5} mol dm^{-3}) λ/nm 227 (ε/dm^3 mol^{-1} cm^{-1} 36,500), 272 (34,400). ESI-MS *m/z* 396.20 $[M+H]^+$ (calc. 396.20). Found C 78.37, H 6.34, N 10.25; required for $C_{26}H_{25}N_3O$ C 78.96, H 6.37, N 10.62.

2.3. Compound **4**

4-Heptyloxybenzaldehyde (2.20 g, 2.23 mL, 10 mmol) was dissolved in EtOH (50 mL). 3-Acetylpyridine (2.42 g, 2.20 mL, 20 mmol) and crushed KOH (1.12 g, 20 mmol) were added to the solution, and then aqueous NH_3 (32%, 38.5 mL) was slowly added. The reaction mixture was stirred at room temperature (ca. 22 °C) overnight and a precipitate formed. This was separated by filtration, washed with EtOH (3 × 10 mL), recrystallized from EtOH and dried *in vacuo*. Compound **4** was isolated as a pale yellow powder (1.22 g, 2.89 mmol, 28.9%). M.p. = 124 °C. ^{1}H NMR (500 MHz, $CDCl_3$): δ/ppm = 9.38 (dd, J = 2.3, 0.8 Hz, 2H, H^{A2}), 8.71 (dd, J = 4.9, 1.7 Hz, 2H, H^{A6}), 8.56 (dt, J = 8.0, 2.3 Hz, 2H, H^{A4}), 7.94 (s, 2H, H^{B3}), 7.71 (m, 2H, H^{C2}), 7.50 (ddd, J = 8.0, 4.9, 0.8 Hz, 2H, H^{A5}), 7.06 (m, 2H, H^{C3}), 4.05 (t, J = 6.6 Hz, 2H, H^{a}), 1.84 (m, 2H, H^{b}), 1.49 (m, 2H, H^{c}), 1.39 (m, 2H, H^{d}), 1.33 (m, 4H, H^{e} + H^{f}), 0.91 (m, 3H, H^{g}). ^{13}C{^{1}H} NMR (500 MHz, $CDCl_3$): δ/ppm = 160.7 (C^{C4}), 155.1 (C^{A3}), 150.7 (C^{B4}), 149.5 (C^{A6}), 147.9 (C^{A2}), 135.3 (C^{A4}), 135.2 (C^{B2}), 130.1 (C^{C1}), 128.5 (C^{C2}), 124.0 (C^{A5}), 117.5 (C^{B3}), 115.4 (C^{C3}), 68.4 (C^{a}), 31.9 (C^{e}), 29.4 (C^{b}), 29.2 (C^{d}), 26.2 (C^{c}), 22.8 (C^{f}), 14.2 (C^{g}). UV-VIS (CH_3CN, 2×10^{-5} mol dm^{-3}) λ/nm 226 (ε/dm^3 mol^{-1} cm^{-1} 35,400), 272 (32,500). ESI-MS *m/z* 424.26 $[M+H]^+$ (calc. 424.23). Found C 79.23, H 6.85, N 9.90; required for $C_{28}H_{29}N_3O$: C 79.40, H 6.90, N 9.92.

2.4. Reaction between **1** and $Cu(OAc)_2·H_2O$: Experiment 1

A solution of $Cu(OAc)_2·H_2O$ (12.0 mg, 0.060 mmol) in MeOH (3 mL) was layered over a $CHCl_3$ solution (3 mL) of **1** (10.2 mg, 0.030 mmol) in a crystallization tube (inner diameter, i.d. = 13.6 mm, volume = 24 mL). Blue block-like crystals were obtained after two months, and one single crystal was selected for X-ray diffraction. Structural determination confirmed the formation of $[Cu_2(\mu\text{-}OAc)_4(\mathbf{1})]_n$. The remaining crystals in the tube were washed with MeOH and $CHCl_3$, dried under vacuum and analyzed by PXRD (see the discussion section).

2.5. Reaction between **1** and $Cu(OAc)_2·H_2O$: Experiment 2

A MeOH (8 mL) solution of $Cu(OAc)_2·H_2O$ (16.3 mg, 0.08 mmol) was layered over a $CHCl_3$ (5 mL) solution of **1** (13.6 mg; 0.04 mmol) in a crystallization tube (i.d. = 13.6 mm, vol. = 24 mL) initially sealed with a septum; after 10 days a syringe-needle was introduced into the septum opening the tube to the air. This was left to stand at room temperature (ca. 22 °C) allowing the blue solution to evaporate in the air for two weeks. The pale blue precipitate that formed was collected by filtration, dried *in vacuo* and then redissolved in MeOH. The blue solution was left to evaporate in the air in an NMR-tube with a septum pierced with a syringe-needle. Light blue block-like crystals visible to the eye were first obtained after three months, and a single crystal was selected for X-ray diffraction after another two months. Structural determination confirmed this to be $\{[Cu_4(\mu_3\text{-}OH)_2(\mu\text{-}OAc)_2(\mu_3\text{-}OAc)_2(AcO\text{-}\kappa O)_2(\mathbf{1})_2]·2MeOH\}_n$. The remaining crystals were washed with MeOH, dried under vacuum and analyzed by PXRD confirming that the single crystal was representative of the bulk material.

2.6. Preparative Scale Reaction between **1** and $Cu(OAc)_2·H_2O$ to Give $[Cu_2(OAc)_4(\mathbf{1})]_n$

Compound **1** (70.0 mg, 0.206 mmol) was dissolved in MeOH (25 mL), then $Cu(OAc)_2·H_2O$ (82.3 mg, 0.412 mmol) was added to the colorless solution. A blue solution was obtained and immediately produced a fine light blue suspension. The solid that formed was collected by filtration and then dried *in vacuo* up to constant weight (4 h). The product was isolated as a light blue powder. Yield for $[Cu_2(OAc)_4(\mathbf{1})]_n$ (79.3 mg, 0.11 mmol, 55%). Found C 50.94, H 4.13, N 5.75; required for $C_{30}H_{29}N_3O_9$: C 51.28, H 4.16, N 5.98. PXRD confirmed the product to be $[Cu_2(OAc)_4(\mathbf{1})]_n$ (see text).

2.7. Crystal Growth of $[2\{Cu_2(\mu\text{-}OAc)_4(\mathbf{2})\}·1.25MeOH]_n$

A solution of $Cu(OAc)_2·H_2O$ (12.0 mg, 0.060 mmol) in MeOH (8 mL) was layered over a $CHCl_3$ solution (5 mL) of **2** (11.4 mg, 0.030 mmol) in a crystallization tube (i.d. = 13.6 mm, vol. = 24 mL). Green block-like crystals grew after two months, and a single crystal was selected for X-ray diffraction. Structural data confirmed a formulation of $[2\{Cu_2(\mu\text{-}OAc)_4(\mathbf{2})\}·1.25MeOH]_n$. The remaining crystals in the tube were washed with MeOH and $CHCl_3$, dried under vacuum and analyzed by PXRD.

2.8. Crystal Growth of $[Cu_2(\mu\text{-}OAc)_4(\mathbf{3})]_n$

A solution of $Cu(OAc)_2·H_2O$ (12.0 mg, 0.060 mmol) in MeOH (3 mL) was layered over a $CHCl_3$ solution (3 mL) of **3** (11.9 mg, 0.030 mmol) in a crystallization tube (i.d. = 13.6 mm, vol. = 24 mL). Blue blocks were obtained after 20 days, and a single crystal was selected for X-ray diffraction. Structural data confirmed a formulation of $[Cu_2(\mu\text{-}OAc)_4(\mathbf{3})]_n$. The remaining crystals in the tube were washed with MeOH and $CHCl_3$, dried under vacuum and analyzed by PXRD.

2.9. Crystal Growth of $[\{Cu_2(\mu\text{-}OAc)_4(\mathbf{4})\}·0.2CHCl_3]_n$

A solution of $Cu(OAc)_2·H_2O$ (12.0 mg, 0.060 mmol) in MeOH (6 mL) was layered over a $CHCl_3$ solution (4 mL) of **4** (12.7 mg, 0.030 mmol) in a crystallization tube (i.d. = 13.6 mm, vol. = 24 mL). Blue plates grew after six months, and a single crystal was selected for X-ray diffraction. This proved to be

$[\{Cu_2(\mu\text{-}OAc)_4(\mathbf{4})\}\cdot 0.2CHCl_3]_n$. The remaining crystals were washed with MeOH and $CHCl_3$, dried under vacuum and analyzed by PXRD.

2.10. Crystallography

Single crystal data were collected on a Bruker APEX-II diffractometer (CuKα radiation) with data reduction, solution and refinement using the programs APEX [35], ShelXT [36], Olex2 [37] and ShelXL v. 2014/7 [38], or using a STOE StadiVari diffractometer equipped with a Pilatus300K detector and with a Metaljet D2 source (GaKα radiation) and solving the structure using Superflip [39,40] and Olex2 [37]. See Sections 2.10–2.15 for details of the radiation type for each structure. The model was refined with ShelXL v. 2014/7 [38]. Structure analysis used Mercury CSD v. 4.1.0 and v. 4.3.0 [41,42].

In $\{[Cu_4(\mu_3\text{-}OH)_2(\mu\text{-}OAc)_2(\mu_3\text{-}OAc)_2(AcO\text{-}\kappa O)_2(\mathbf{1})_2]\cdot 2MeOH\}_n$, the disordered MeOH molecules have been modelled over several fractional-occupancy sites. In $[\{Cu_2(\mu\text{-}OAc)_4(\mathbf{4})\}\cdot 0.2CHCl_3]_n$, the *n*-heptyl chain was disordered and was modelled over two sites of fractional occupancies 0.8 and 0.2; the minor occupancy site for the *n*-heptyl chain is associated with a partial occupancy $CHCl_3$ molecule. The relatively high R-factor for $[Cu_2(\mu\text{-}OAc)_4(\mathbf{1})]_n$ is due to the sharp drop in the intensity of the diffraction as a function of the resolution.

Powder X-ray diffraction (PXRD) patterns were collected at room temperature in transmission mode using a Stoe Stadi P diffractometer equipped with a Cu Kα1 radiation (Ge(111) monochromator) and a DECTRIS MYTHEN 1K detector. The reflections of the bulk samples of $[\{Cu_4(\mu_3\text{-}OH)_2(\mu\text{-}OAc)_2(\mu_3\text{-}OAc)_2(AcO\text{-}\kappa O)_2(\mathbf{1})_2\}\cdot 2MeOH]_n$ and $[Cu_2(\mu\text{-}OAc)_4(\mathbf{3})]_n$ were indexed with the monoclinic cells *C*2/*c* and $P2_1/n$, respectively. The reflections of the bulk samples of $[2\{Cu_2(\mu\text{-}OAc)_4(\mathbf{2})\}\cdot 1.25MeOH]_n$ and $[\{Cu_2(\mu\text{-}OAc)_4(\mathbf{4})\}\cdot 0.2CHCl_3]_n$ and the crystalline material from the preparative scale synthesis of $[Cu_2(\mu\text{-}OAc)_4(\mathbf{1})]_n$ were indexed with the triclinic cell *P*–1. For $[\{Cu_4(\mu_3\text{-}OH)_2(\mu\text{-}OAc)_2(\mu_3\text{-}OAc)_2(AcO\text{-}\kappa O)_2(\mathbf{1})_2\}\cdot 2MeOH]_n$ and $[Cu_2(\mu\text{-}OAc)_4(\mathbf{3})]_n$, Rietveld refinement analysis [43] was carried out, while for $[2\{Cu_2(\mu\text{-}OAc)_4(\mathbf{2})\}\cdot 1.25MeOH]_n$, the preparative scale synthesis of $[Cu_2(\mu\text{-}OAc)_4(\mathbf{1})]_n$ and $[\{Cu_2(\mu\text{-}OAc)_4(\mathbf{4})\}\cdot 0.2CHCl_3]_n$, whole-pattern decomposition (profile matching) analysis [44–46] of the diffraction patterns was performed with the package FULLPROF SUITE [46,47] (version July-2019) using a previously determined instrument resolution function based on a NIST640d standard. The structural models were taken from the single crystal X-ray diffraction refinements. Refined parameters in Rietveld were: Scale factor, zero shift, lattice parameters, Cu atomic positions, background points and peaks shapes as a Thompson-Cox-Hastings pseudo-Voigt function. Preferred orientations as a March-Dollase multi-axial phenomenological model were incorporated into the analysis. The refinements confirmed that the bulk materials of $[\{Cu_4(\mu_3\text{-}OH)_2(\mu\text{-}OAc)_2(\mu_3\text{-}OAc)_2(AcO\text{-}\kappa O)_2(\mathbf{1})_2\}\cdot 2MeOH]_n$ and $[Cu_2(\mu\text{-}OAc)_4(\mathbf{3})]_n$ are representative of the analyzed single crystals.

Refined parameters in Profile matching were: Zero shift, lattice parameters, peak asymmetry, sample transparency, and peaks shapes as a Thompson-Cox-Hastings pseudo-Voigt function. The refinements confirmed that the bulk samples of $[2\{Cu_2(\mu\text{-}OAc)_4(\mathbf{2})\}\cdot 1.25MeOH]_n$, the preparative scale synthesis of $[Cu_2(\mu\text{-}OAc)_4(\mathbf{1})]_n$ and $[\{Cu_2(\mu\text{-}OAc)_4(\mathbf{4})\}\cdot 0.2CHCl_3]_n$ are representative of the analyzed single crystals, but all show some minor impurities.

2.11. $[Cu_2(\mu\text{-}OAc)_4(\mathbf{1})]_n$

$C_{30}H_{29}Cu_2N_3O_9$, M_r = 702.64, blue block, triclinic, space group *P*–1, *a* = 8.4817(5), *b* = 13.7510(10), *c* = 15.3776(10) Å, α = 115.153(5), β = 104.720(5), γ = 92.942(5)°, *V* = 1543.94(19) Å^3, D_c = 1.511 g cm^{-3}, *T* = 130 K, *Z* = 2, *Z*′ = 1, μ(GaKα) = 7.754 mm^{-1}. Total 23704 reflections, 6163 unique (R_{int} = 0.1083). Refinement of 3838 reflections (402 parameters) with $I > 2\sigma(I)$ converged at final R_1 = 0.1432 (R_1 all data = 0.2081), wR_2 = 0.3804 ($wR2$ all data = 0.4385), gof = 1.601. CCDC 1967918.

2.12. $[\{Cu_4(\mu_3\text{-}OH)_2(\mu\text{-}OAc)_2(\mu_3\text{-}OAc)_2(AcO\text{-}\kappa O)_2(\mathbf{1})_2\}\cdot 2MeOH]_n$

$C_{58}H_{62}Cu_4N_6O_{18}$, M_r = 1385.29, blue block, monoclinic, space group *C*2/*c*, a = 26.904(2), b = 16.9697(15), c = 14.2030(13) Å, β = 107.436(3)°, V = 6186.4(10) Å^3, D_c = 1.487 g cm^{-3}, T = 130 K, Z = 4, Z' = 0.5, μ(CuKα) = 2.175 mm^{-1}. Total 25907 reflections, 5690 unique (R_{int} = 0.0369). Refinement of 5278 reflections (445 parameters) with $I > 2\sigma(I)$ converged at final R_1 = 0.0421 (R_1 all data = 0.0446), wR_2 = 0.1253 ($wR2$ all data = 0.1275), gof = 1.089. CCDC 1967916.

2.13. $[2\{Cu_2(\mu\text{-}OAc)_4(\mathbf{2})\}\cdot 1.25MeOH]_n$

$C_{67.25}H_{75}Cu_4N_6O_{19.25}$, M_r = 1529.49, green block, triclinic, space group *P*–1, a = 14.2771(16), b = 16.0424(18), c = 17.258(2) Å, α = 109.126(3), β = 92.317(3), γ = 110.953(3)°, V = 3431.5(7) Å^3, D_c = 1.480 g cm^{-3}, T = 130 K, Z = 2, Z' = 1, μ(Cu$K\alpha$) = 2.032 mm^{-1}. Total 61235 reflections, 12421 unique (R_{int} = 0.0237). Refinement of 12194 reflections (886 parameters) with $I > 2\sigma(I)$ converged at final R_1 = 0.0347 (R_1 all data = 0.0352), wR_2 = 0.0977 ($wR2$ all data = 0.0980), gof = 1.049. CCDC 1967920.

2.14. $[Cu_2(\mu\text{-}OAc)_4(\mathbf{3})]_n$

$C_{34}H_{37}Cu_2N_3O_9$, M_r = 758.74, blue block, monoclinic, space group $P2_1/n$, a = 11.0414(3), b = 21.6148(5), c = 14.4787(3) Å, β = 106.004(2)°, V = 3321.53(14) Å^3, D_c = 1.517 g cm^{-3}, T = 130 K, Z = 4, Z' = 1, μ(Ga$K\alpha$) = 7.237 mm^{-1}. Total 52984 reflections, 6665 unique (R_{int} = 0.0729). Refinement of 6294 reflections (438 parameters) with $I > 2\sigma(I)$ converged at final R_1 = 0.0805 (R_1 all data = 0.0867), wR_2 = 0.1549 (wR_2 all data = 0.1578), gof = 1.163. CCDC 1967919.

2.15. $[\{Cu_2(\mu\text{-}OAc)_4(\mathbf{4})\}\cdot 0.2CHCl_3]_n$

$C_{36.2}H_{41.2}Cl_{0.6}Cu_2N_3O_9$, M_r = 810.67, blue plate, triclinic, space group *P*–1, a = 8.3686(6), b = 14.7025(11), c = 16.4640(13) Å, α = 73.217(4), β = 78.314(4), γ = 73.555(4)°, V = 1843.9(2) Å^3, D_c = 1.460 g cm^{-3}, T = 130 K, Z = 2, Z' = 1, μ(Cu$K\alpha$) = 2.302 mm^{-1}. Total 21215 reflections, 6656 unique (R_{int} = 0.0353). Refinement of 5906 reflections (492 parameters) with $I > 2\sigma(I)$ converged at final R_1 = 0.0514 (R_1 all data = 0.0566), wR_2 = 0.1495 ($wR2$ all data = 0.1553), gof = 1.048. CCDC 1967917.

3. Results and Discussion

3.1. Synthesis and Characterization of Ligands **3** and **4**

Compounds **3** and **4** were synthesized using Hanan's [48] one-pot synthesis from 3-acetylpyridine and the appropriate 4-alkyloxybenzaldehyde in the presence of base, followed by the addition of aqueous ammonia. After purification, **3** and **4** were isolated as white solids in yields of 23.5 and 28.9%, respectively. Figures S1 and S2 (see Supplementary Materials) show the electrospray mass spectra of **3** and **4**, with base peaks at *m*/*z* = 396.20 and 424.26, respectively, corresponding to the $[M+H]^+$ ions. The solid-state IR spectra of **3** and **4** are similar (Figures S3 and S4), consistent with **3** and **4** having analogous structures. The ^{1}H and ^{13}C{^{1}H} NMR spectra were assigned using 2D methods. Figure 1 displays a comparison of the ^{1}H NMR spectra of the two compounds with the only significant difference being in the aliphatic region consistent with an *n*-pentyloxy chain in **3** versus *n*-heptyloxy chain in **4**. The HMQC and HMBC spectra are shown in Figures S5–S8.

The high-energy bands in the solution absorption spectra of **3** and **4** (Figure 2) arise from spin-allowed $\pi^*\leftarrow n$, and $\pi^*\leftarrow\pi$ transitions, and the spectra have the same profile as those of the methoxy, ethoxy and *n*-butoxy derivatives [33,34].

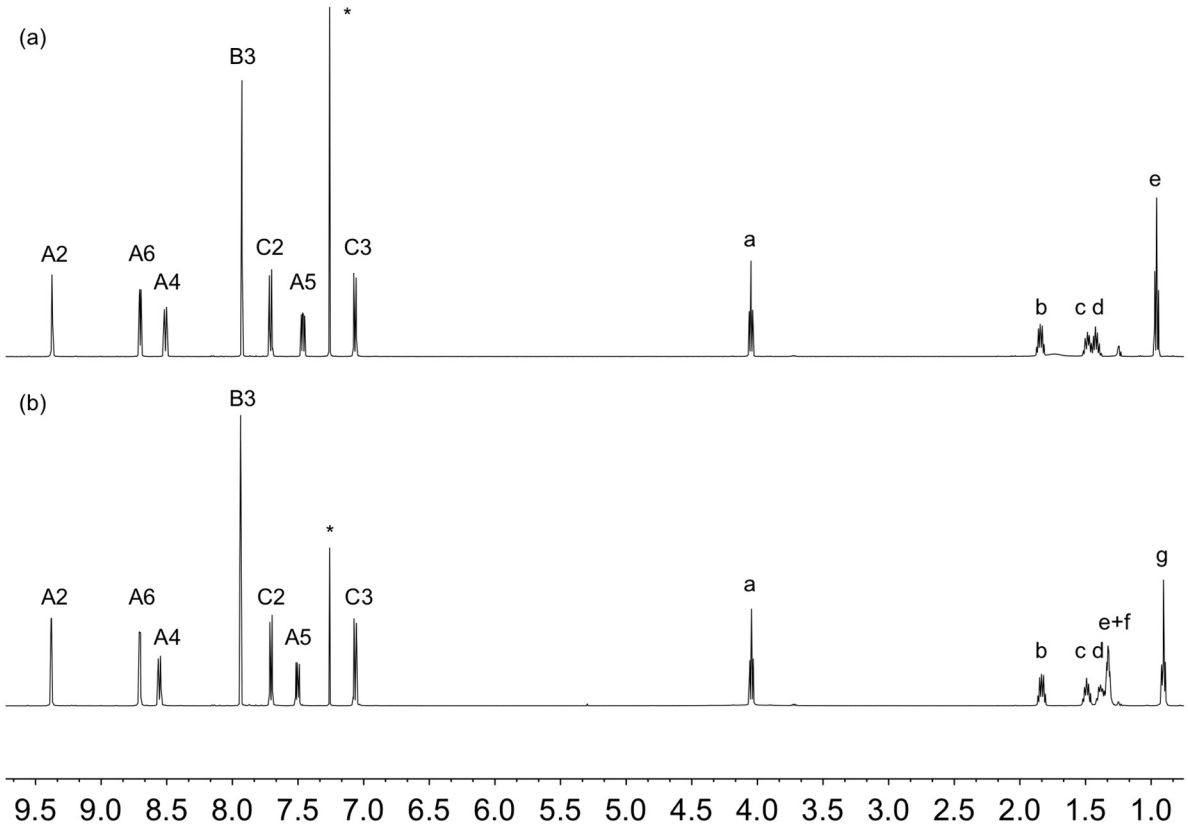

Figure 1. The ^{1}H (500 MHz, $CDCl_3$, 298 K) NMR spectra of (**a**) **3** and (**b**) **4**. * = residual $CHCl_3$. See Scheme 4 for atom labelling.

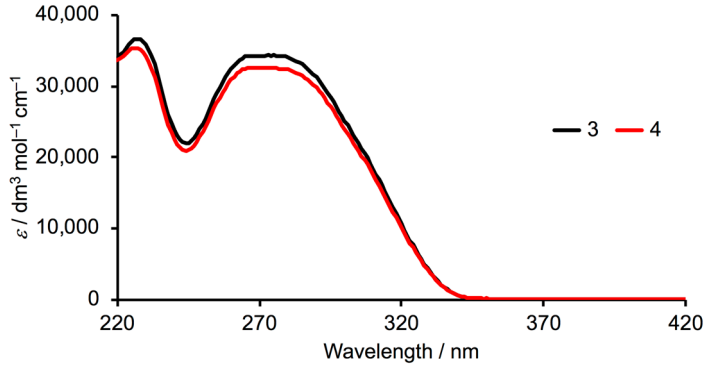

Figure 2. Solution absorption spectra of compounds **3** and **4** (MeCN, 2×10^{-5} mol dm^{-3}).

3.2. *Reactions of Copper(II) Acetate with Ligand* **1**

A series of reactions were carried out between **1** and $Cu(OAc)_2{\cdot}H_2O$, and the differences in conditions and the outcomes of the reactions are summarized in Scheme 5. All reactions were carried out in air at room temperature (ca. 22 °C). With the anticipation of the formation of dinuclear paddle-wheel units, crystallization tubes were prepared with a 2:1 molar ratio of $Cu(OAc)_2{\cdot}H_2O$:**1**, dissolved in MeOH and $CHCl_3$, respectively. The tubes were left to stand at ambient temperature. Blue blocks of $[Cu_2(\mu\text{-}OAc)_4(\mathbf{1})]_n$ suitable for single-crystal X-ray diffraction were obtained after two months from experiment 1 (see Section 2.4). In some tubes (experiment 2, Section 2.5), the solvent was allowed to evaporate more quickly by exposure to air and a precipitate formed. After filtration, the precipitate was redissolved in MeOH and the solution left to stand at room temperature. After several months, X-ray quality blue crystals were collected, and structural determination showed the formation

of {[$Cu_4(\mu_3\text{-}OH)_2(\mu\text{-}OAc)_2(\mu_3\text{-}OAc)_2(AcO\text{-}\kappa O)_2(\mathbf{1})_2$]·2MeOH}$_n$. The remainder of the crystals from both Experiments 1 and 2 were collected and analyzed by PXRD. In both cases, PXRD (Figure 3a,b) confirmed that the bulk materials from the crystal growth experiments carried out over several months corresponded to {[$Cu_4(\mu_3\text{-}OH)_2(\mu\text{-}OAc)_2(\mu_3\text{-}OAc)_2(AcO\text{-}\kappa O)_2(\mathbf{1})_2$]·2MeOH}$_n$.

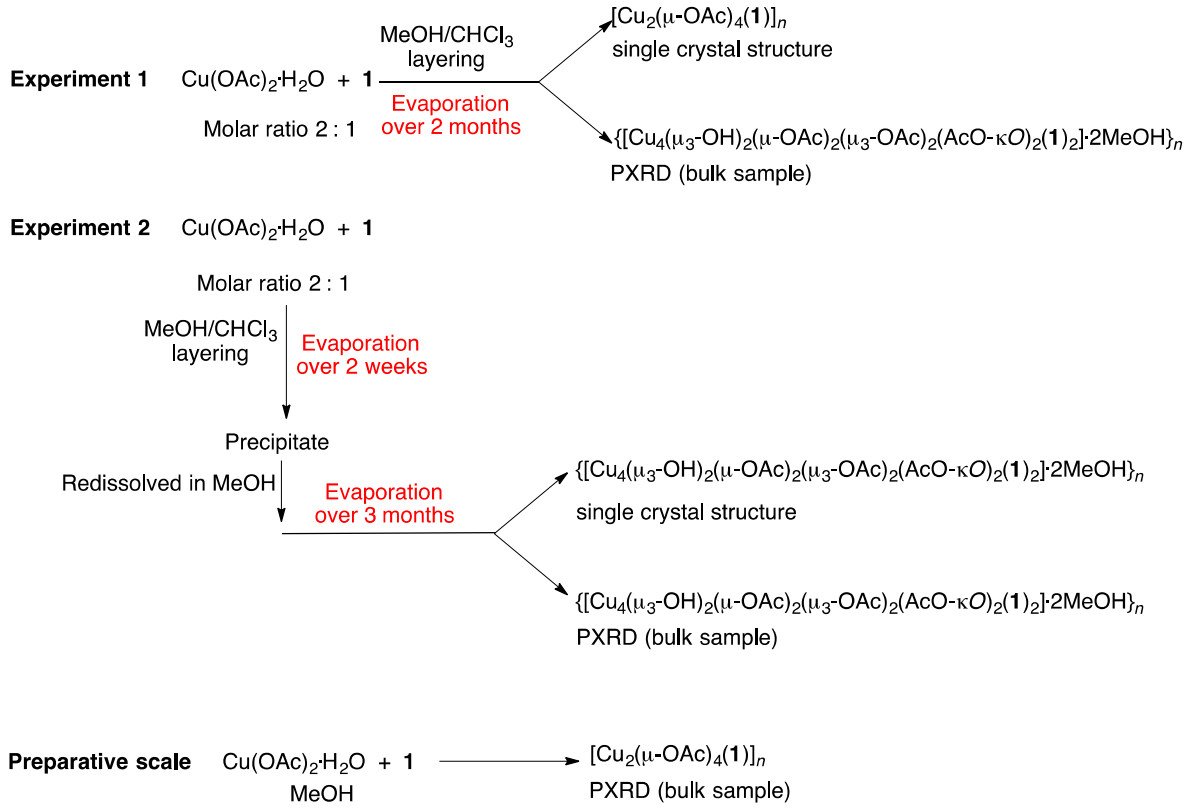

Scheme 5. Summary of the reactions of ligand **1** with $Cu(OAc)_2{\cdot}H_2O$. Crystal growths by layering (experiments 1 and 2) and the preparative scale reactions were carried out in air at ambient temperature.

A preparative scale reaction of $Cu(OAc)_2{\cdot}H_2O$ and **1** (2:1 molar ratio) was carried out in MeOH and a pale-blue solid immediately formed. Exposure to air and moisture, in this case, was minimal. The sample was dried, and elemental analysis was in agreement with a stoichiometry of $Cu(OAc)_2(\mathbf{1})$, and PXRD (Figure 3c) was consistent with the material being [$Cu_2(\mu\text{-}OAc)_4(\mathbf{1})$]$_n$.

The results indicate that, on a preparative scale, ligand **1** reacts with $Cu(OAc)_2{\cdot}H_2O$ to immediately yield the 1D-coordination polymer [$Cu_2(\mu\text{-}OAc)_4(\mathbf{1})$]$_n$. However, when the reaction is carried out under conditions of crystal growth by layering over a period of several months, the incorporation of hydroxido ligands and formation of {$Cu_4(\mu_3\text{-}OH)_2(OAc)_6$}-clusters becomes dominant. PXRD reveals that the double-stranded coordination polymer {[$Cu_4(\mu_3\text{-}OH)_2(\mu\text{-}OAc)_2(\mu_3\text{-}OAc)_2(AcO\text{-}\kappa O)_2(\mathbf{1})_2$]·2MeOH}$_n$ is the major product in both experiments 1 and 2, and the selection of the single crystal of [$Cu_2(\mu\text{-}OAc)_4(\mathbf{1})$]$_n$ was fortuitous.

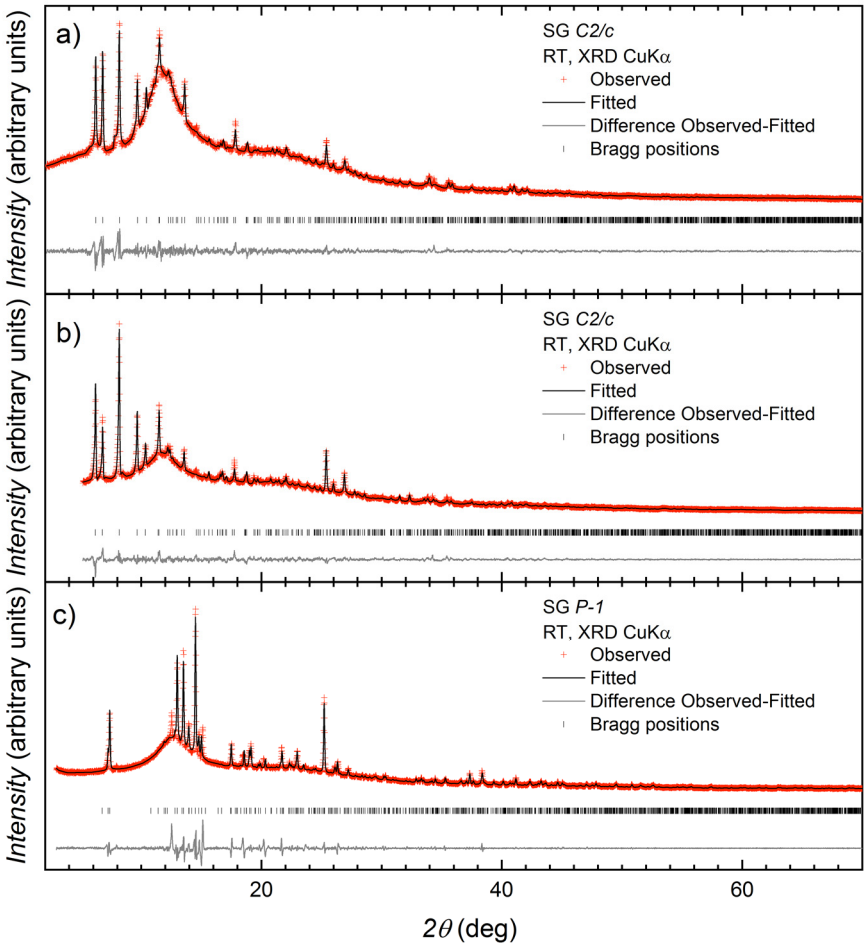

Figure 3. Laboratory X-ray diffraction (CuKα1 radiation) pattern (red crosses) of (**a**) the bulk crystalline material from experiment 2 with fitting to the predicted pattern from the single crystal determination of $[\{Cu_4(\mu_3\text{-}OH)_2(\mu\text{-}OAc)_2(\mu_3\text{-}OAc)_2(AcO\text{-}\kappa O)_2(\mathbf{1})_2\}\cdot 2MeOH]_n$; (**b**) the bulk crystalline material from experiment 1 with fitting to the predicted pattern from the single crystal determination of $[\{Cu_4(\mu_3\text{-}OH)_2(\mu\text{-}OAc)_2(\mu_3\text{-}OAc)_2(AcO\text{-}\kappa O)_2(\mathbf{1})_2\}\cdot 2MeOH]_n$; and (**c**) the crystalline material from the preparative scale synthesis with fitting to the predicted pattern from the single crystal determination of $[Cu_2(\mu\text{-}OAc)_4(\mathbf{1})]_n$ at room temperature. The black line corresponds to the best fit from the profile matching refinement. Lower vertical marks denote the Bragg peak positions. The bottom line in each plot represents the difference between experimental and calculated points.

The IR spectra of the bulk materials from experiments 1 and 2 compared to the spectrum of the product of the preparative reaction of **1** with $Cu(OAc)_2\cdot H_2O$ are consistent with the conclusions drawn from the PXRD. Figure 4a shows an expansion of the region below 1760 cm^{-1} in the IR spectra of the bulk samples from experiments 1 and 2 confirming that the materials are the same, i.e., $[\{Cu_4(\mu_3\text{-}OH)_2(\mu\text{-}OAc)_2(\mu_3\text{-}OAc)_2(AcO\text{-}\kappa O)_2(\mathbf{1})_2\}\cdot 2MeOH]_n$. Full spectra are shown in Figure S9 and the absorption observed at 3420 cm^{-1} is likely to arise from the O–H stretch of the hydroxido ligands [49,50]. A comparison of the IR spectra of the bulk sample from experiment 1 with that of the product from the preparative scale reaction of **1** with $Cu(OAc)_2\cdot H_2O$ is shown in Figure 4b. The absorption at 916 cm^{-1} present in the spectrum of $[\{Cu_4(\mu_3\text{-}OH)_2(\mu\text{-}OAc)_2(\mu_3\text{-}OAc)_2(AcO\text{-}\kappa O)_2(\mathbf{1})_2\}\cdot 2MeOH]_n$ (Figure 4a and black line in Figure 4b) is tentatively assigned to a vibrational mode of the μ_3-OH group [51]. The band at 3420 cm^{-1} present in the spectrum of $[\{Cu_4(\mu_3\text{-}OH)_2(\mu\text{-}OAc)_2(\mu_3\text{-}OAc)_2(AcO\text{-}\kappa O)_2(\mathbf{1})_2\}\cdot 2MeOH]_n$ is absent in the IR spectrum of $[Cu_2(\mu\text{-}OAc)_4(\mathbf{1})]_n$.

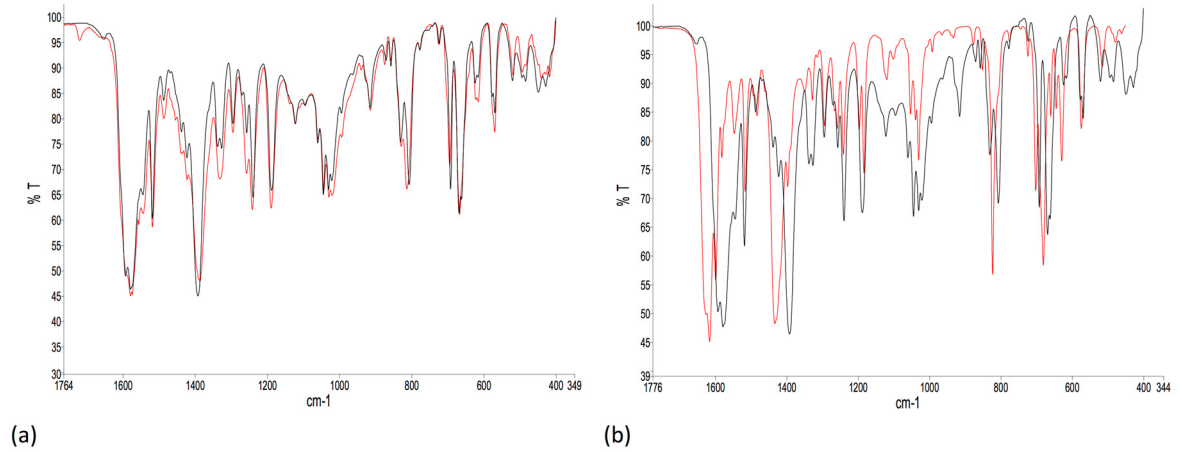

Figure 4. Normalized FT-IR spectra (solid-state) of the bulk materials from (**a**) experiment 1 (black line) and experiment 2 (red line), and (**b**) experiment 1 (black line, $[\{Cu_4(\mu_3\text{-}OH)_2(\mu\text{-}OAc)_2(\mu_3\text{-}OAc)_2(AcO\text{-}\kappa O)_2(\mathbf{1})_2\}\cdot 2MeOH]_n$) and the preparative scale reaction (red line, $[Cu_2(\mu\text{-}OAc)_4(\mathbf{1})]_n$). Full spectra are given in Figure S9.

3.3. Crystal Structure of $[Cu_2(\mu\text{-}OAc)_4(\mathbf{1})]_n$

$[Cu_2(\mu\text{-}OAc)_4(\mathbf{1})]_n$ crystallizes in the triclinic space group *P*–1 and features $\{Cu_2(\mu\text{-}OAc)_4\}$ paddle-wheel units connecting ligands **1** (Figure 5). An ORTEP-style diagram of the asymmetric unit is depicted in Figure S10 (see Supplementary Materials) and Cu–N and Cu–O bond lengths are given in Table 1. Ligand **1** adopts conformation 1 in Scheme 2, resulting in a zigzag 1D chain (Figure 5). In this and the other structures described in this work, the central pyridine ring is non-coordinating. The 3,2′:6′,3″-unit is close to planar with angles between the least squares mean planes of the pyridine rings containing N1/N2 and N2/N3 being 11.1 and 17.5°, respectively. The phenyl ring is twisted only 19.5° out of the plane of the central pyridine ring. The near-planarity is a consequence of the head-to-tail stacking of the 4′-(4-methoxyphenyl)pyridine units in adjacent chains (Figure 6a). The stacked phenyl rings are offset, and although the inter-plane separation of 4.15 Å and centroid … centroid separation of 4.65 Å are larger than is ideal for face-to-face π-stacking [52], the interaction is augmented by $CH_{MeO} \cdots \pi_{pyridine}$ contacts (CH … centroid = 2.91 Å). Along a 1D polymer chain, ligands **1** lie on alternate sides of the chain and extension of the stacking interactions depicted in Figure 6a leads to the formation of 2D sheets (Figure 6b). Figure 6c illustrates that two of the four acetato ligands of each $\{Cu_2(\mu\text{-}OAc)_4\}$ unit are accommodated in cavities in an adjacent sheet. An important detail with respect to the structures discussed in later sections is that the methoxy group is accommodated within the pocket of a 3,2′:6′,3″-tpy domain in the adjacent chain (Figure 6d). The closest $H_{MeO} \cdots H_{tpy}$ distances are 2.3 and 2.8 Å. The overall efficiency of the packing in $[Cu_2(\mu\text{-}OAc)_4(\mathbf{1})]_n$ is demonstrated by the lack of any solvent of crystallization.

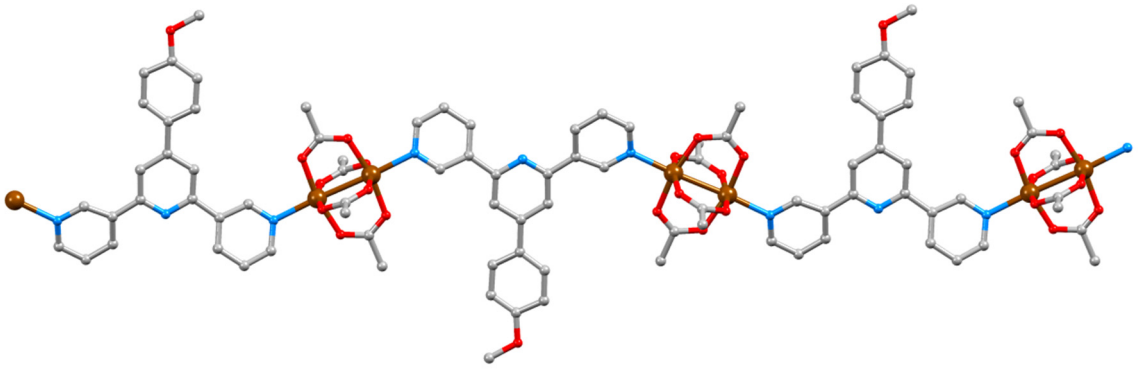

Figure 5. Part of one chain in $[Cu_2(\mu\text{-}OAc)_4(\mathbf{1})]_n$.

Table 1. Selected bond lengths in the {Cu_2(μ-OAc)$_4$}-containing coordination polymers.

Coordination Polymer	Cu–O/Å	Cu–N/Å
[Cu_2(μ-OAc)$_4$(**1**)]$_n$	1.964(8), 1.977(8), 1.987(9), 1.987(9), 1.943(8), 1.984(9), 1.953(9), 1.965(9)	2.150(9), 2.156(8)
[2{Cu_2(μ-OAc)$_4$(**2**)}·1.25MeOH]$_n$	1.9659(16), 1.9764(16), 1.9728(15), 1.9777(16), 1.9786(15), 1.9803(15), 1.9753(15), 1.9544(15), 1.9805(16), 1.9671(15), 1.9971(15), 1.9580(15), 1.9745(16), 1.9808(15), 1.9716(16), 1.9839(15)	2.1672(18), 2.1717(17), 2.1875(17), 2.1709(17)
[Cu_2(μ-OAc)$_4$(**3**)]$_n$	1.964(4), 1.992(4), 1.959(4), 1.988(4), 1.951(4), 1.950(4), 1.992(4), 1.997(4)	2.205(4), 2.161(4)
[{Cu_2(μ-OAc)$_4$(**4**)}·0.2$CHCl_3$]$_n$	1.963(2), 1.967(2), 1.976(2), 1.976(2), 1.976(2), 1.974(2), 1.982(2), 1.972(2)	2.163(3), 2.149(3)

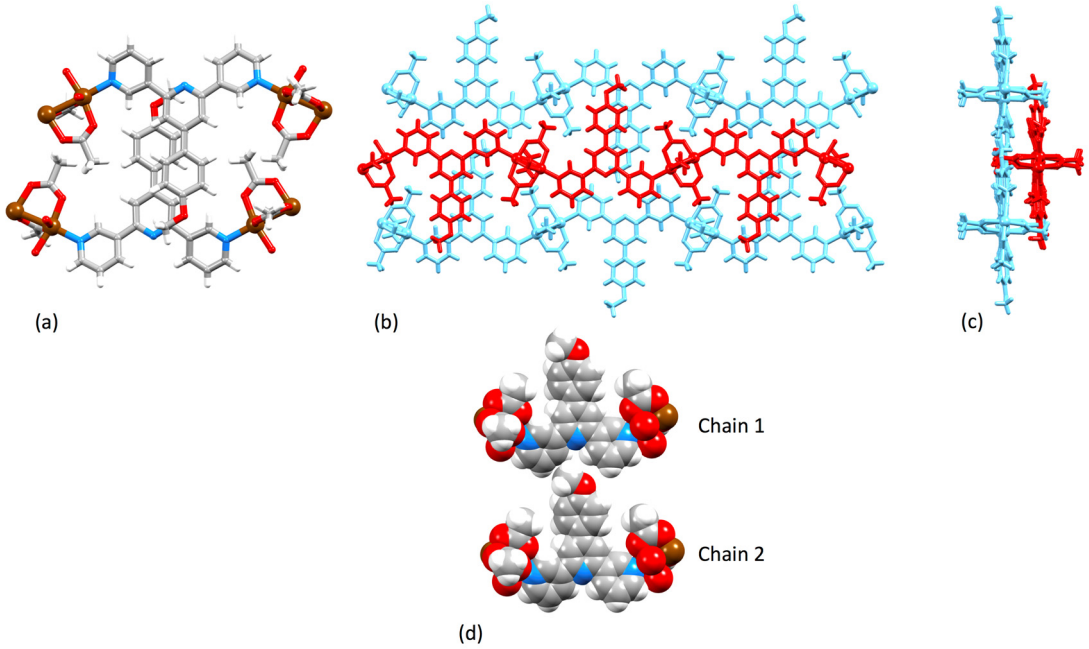

Figure 6. Packing in [Cu_2(μ-OAc)$_4$(**1**)]$_n$: (**a**) Head-to-tail stacking of 4′-(4-methoxyphenyl)pyridine units in adjacent chains; (**b**) extended stacking interactions lead to the formation of 2D sheets – the red and blue chains lie in adjacent sheets; (**c**) an orthogonal view of diagram (**b**) showing the accommodation of acetato ligands in cavities in the adjacent sheet; (**d**) accommodation of a methoxy group in one chain in the pocket of a 3,2′:6′,3″-tpy domain in an adjacent chain.

It is pertinent to compare the 1D-coordination polymer chains in [Cu_2(μ-OAc)$_4$(**1**)]$_n$ and [Zn_2(μ-OAc)$_4$(**1a**)]$_n$ in which **1a** = 4′-(4-alkyloxyphenyl)-4,2′:6′,4″-tpy [20]. The overlay, shown in Figure 7, emphasizes the change in the vectorial arrangement of the outer pyridine-ring nitrogen lone pairs and the consequential effect on the backbone of the zigzag chain.

Changes to the crystallization and work-up conditions (see Materials and Method section and Section 3.2) resulted in the growth of blue crystals of {[Cu_4(μ_3-OH)$_2$(μ-OAc)$_2$(μ_3-OAc)$_2$(AcO-κ*O*)$_2$(**1**)$_2$]·2MeOH}$_n$. This 1D coordination polymer crystallizes in the monoclinic space group *C*2/*c* and consists of ligands **1** (in conformation 2 in Scheme 2) linked by tetranuclear copper clusters. The asymmetric unit is depicted in Figure S11 and contains one independent ligand **1** and half of a copper cluster; the second half is generated by inversion. Consequently, the polymer is double-stranded, as shown in Figure 8a. The cluster (Figure 8b) comprises a planar array of four Cu atoms with Cu … Cu edge lengths of 3.3770(6) and

3.0822(7) Å. Two μ_3-OH ligands (Cu–O = 1.9429(17), 1.9942(18)Å) support the rhombus (Figure 8b) and the Cu … Cu separation for the unique doubly bridged unit is 2.9863(7) Å. The hydroxido H atom was directly located (O–H = 0.841(18) Å). The edges of the Cu_4 unit are bridged by two μ-acetato (Cu–O = 1.9406(19), 2.186(2) Å) and two μ_3-acetato (Cu–O = 1.9879(19), 2.453(2), 2.688(2) Å) ligands; for the bridging descriptors, we consider the long Cu–O length of 2.688(2) Å to be a bonding interaction. Atom Cu2 is further coordinated by a monodentate acetato ligand (Cu–O = 1.965(2) Å). The coordination numbers of Cu1 and Cu2 are, therefore, six and five, respectively. A search of the CSD (v. 5.41 [53]) for copper clusters containing a $\{Cu_4(\mu_3\text{-}OH)_2(\mu\text{-}OAc)_2\}$ with the same geometry as that in $\{[Cu_4(\mu_3\text{-}OH)_2(\mu\text{-}OAc)_2(\mu_3\text{-}OAc)_2(AcO\text{-}\kappa O)_2(\mathbf{1})_2]\cdot 2MeOH\}_n$ revealed 75 hits, but none identical to that shown in Figure 8b. Examples of closely related clusters include those with CSD refcodes IWAHAP [54], MAFBUR [55], DUYWOL [56] and QAWHUS [57].

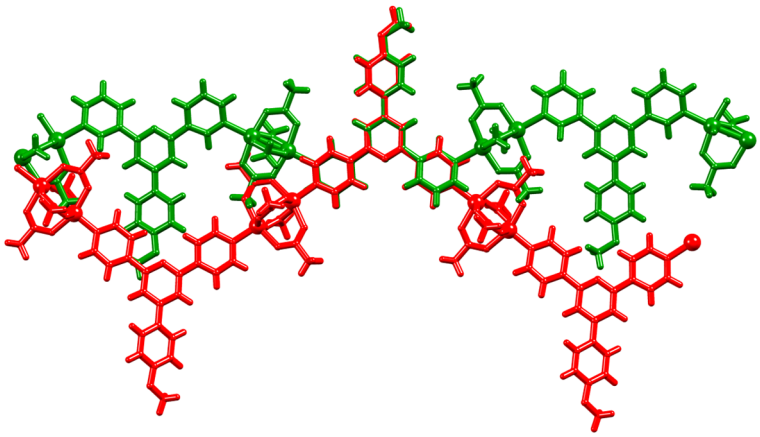

Figure 7. Overlay of parts of the 1D-coordination polymer chains in $[Cu_2(\mu\text{-}OAc)_4(\mathbf{1})]_n$ (green) and $[Zn_2(\mu\text{-}OAc)_4(\mathbf{1a})]_n$ (red). The Cambridge Structural Database, CSD [53], refcode for $[Zn_2(\mu\text{-}OAc)_4(\mathbf{1a})]_n$ is SOXSEF.

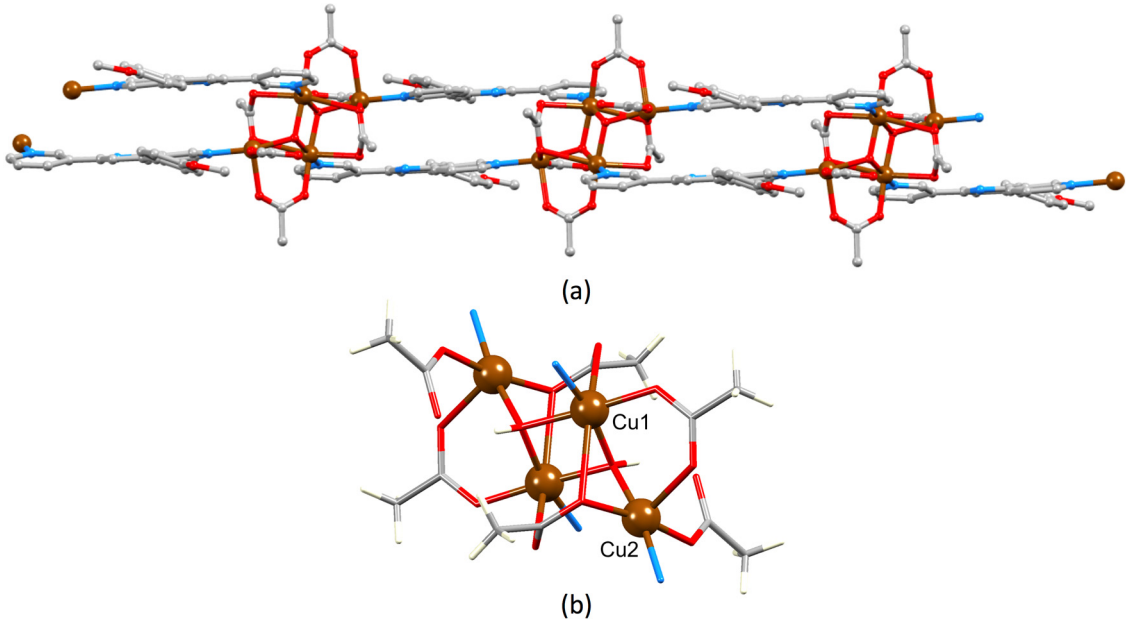

Figure 8. (**a**) Part of one double-stranded chain (solvent omitted) and (**b**) the cluster unit in $\{[Cu_4(\mu_3\text{-}OH)_2(\mu\text{-}OAc)_2(\mu_3\text{-}OAc)_2(AcO\text{-}\kappa O)_2(\mathbf{1})_2]\cdot 2MeOH\}_n$.

In the double-stranded chain, ligands **1** in adjacent strands lie over one another, but in an offset manner. This is illustrated in Figure 9a with green and orange coding. Pairs of 4-methoxyphenyl units engage in π-stacking with a centroid … centroid separation of 3.99 Å and an angle between the ring-planes of 8.7°. In the 3,2′:6′,3″-tpy unit, only the ring containing N2 is involved in face-to-face π-stacking; pyridine rings containing N2 and N2^{i} (symmetry code i = 1–*x*, *y*, $^{3}/_{2}$–*z*) stack with a centroid … centroid distance of 3.69 Å and an angle between the ring-planes of 9.7° (Figure 9a,b). π-Stacking interactions also occur between polymer chains to give extended interactions through the lattice (Figure S12 in Supplementary Materials).

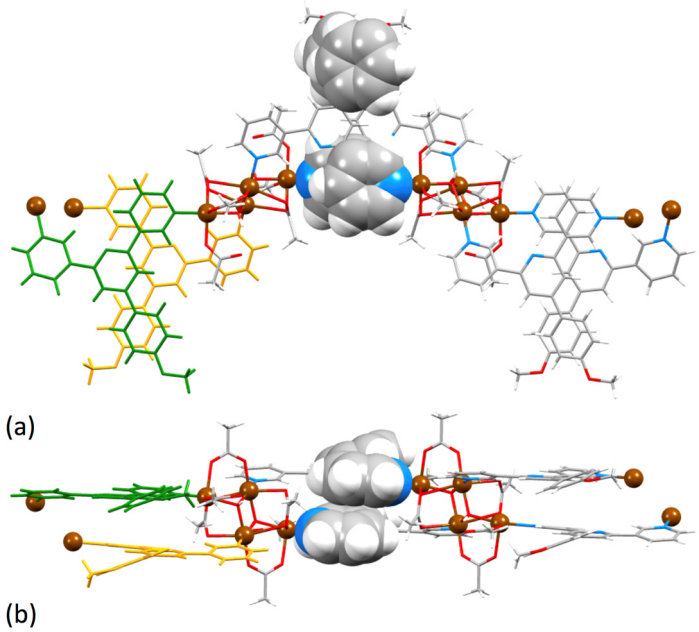

Figure 9. (**a**) Part of one double-stranded chain in {[Cu_4(μ$_3$-OH)$_2$(μ-OAc)$_2$(μ$_3$-OAc)$_2$(AcO-κ*O*)$_2$(**1**)$_2$]·2MeOH}$_n$ (solvent omitted) showing π-stacking of pairs of phenyl and pairs of pyridine rings (space-filling representation) an, in green and orange, the relative orientations of stacked ligands **1**. (**b**) The chain in diagram (a) viewed through the double-strand.

3.4. Reactions of Copper(II) Acetate with Ligands **2**, **3** *and* **4**

Methanol solutions of $Cu(OAc)_2·H_2O$ layered over $CHCl_3$ solutions of **2**, **3** or **4** with a 2:1 molar ratio of $Cu(OAc)_2·H_2O$:ligand yielded blue crystals. After the selection of single crystals for structure determination, the remaining crystals were analyzed by powder diffraction. PXRD refinements confirmed that the bulk material was representative of the analyzed single crystal (Figure 10a–c).

The compounds [2{Cu_2(μ-OAc)$_4$(**2**)}·1.25MeOH]$_n$ and [{Cu_2(μ-OAc)$_4$(**4**)}·0.2$CHCl_3$]$_n$ crystallize in the triclinic space group *P*–1, while [Cu_2(μ-OAc)$_4$(**3**)]$_n$ crystallizes in the monoclinic space group $P2_1/n$. All three compounds are 1D coordination polymers with the 4′-substituted 3,2′:6′,3″-tpy ligands linking {Cu_2(μ-OAc)$_4$} paddle-wheel units. The asymmetric units of the structures are shown in Figures S13–S15. In [2{Cu_2(μ-OAc)$_4$(**2**)}·1.25MeOH]$_n$, there are two independent ligands and two independent {Cu_2(μ-OAc)$_4$} units. In the latter, the Cu–O bond lengths lie in the range 1.9544(15)–1.9971(15) Å (Table 1) and the geometries of the paddle-wheel units are similar. The crystallographically independent ligands **2** differ in the conformations of the *n*-butyl chains, only one is fully extended. Cu–O and Cu–N bond lengths for all three structures are given in Table 1 and are unexceptional. The alkyloxy chains in [{Cu_2(μ-OAc)$_4$(**4**)}·0.2$CHCl_3$]$_n$ and [Cu_2(μ-OAc)$_4$(**3**)]$_n$ are in partly extended conformations.

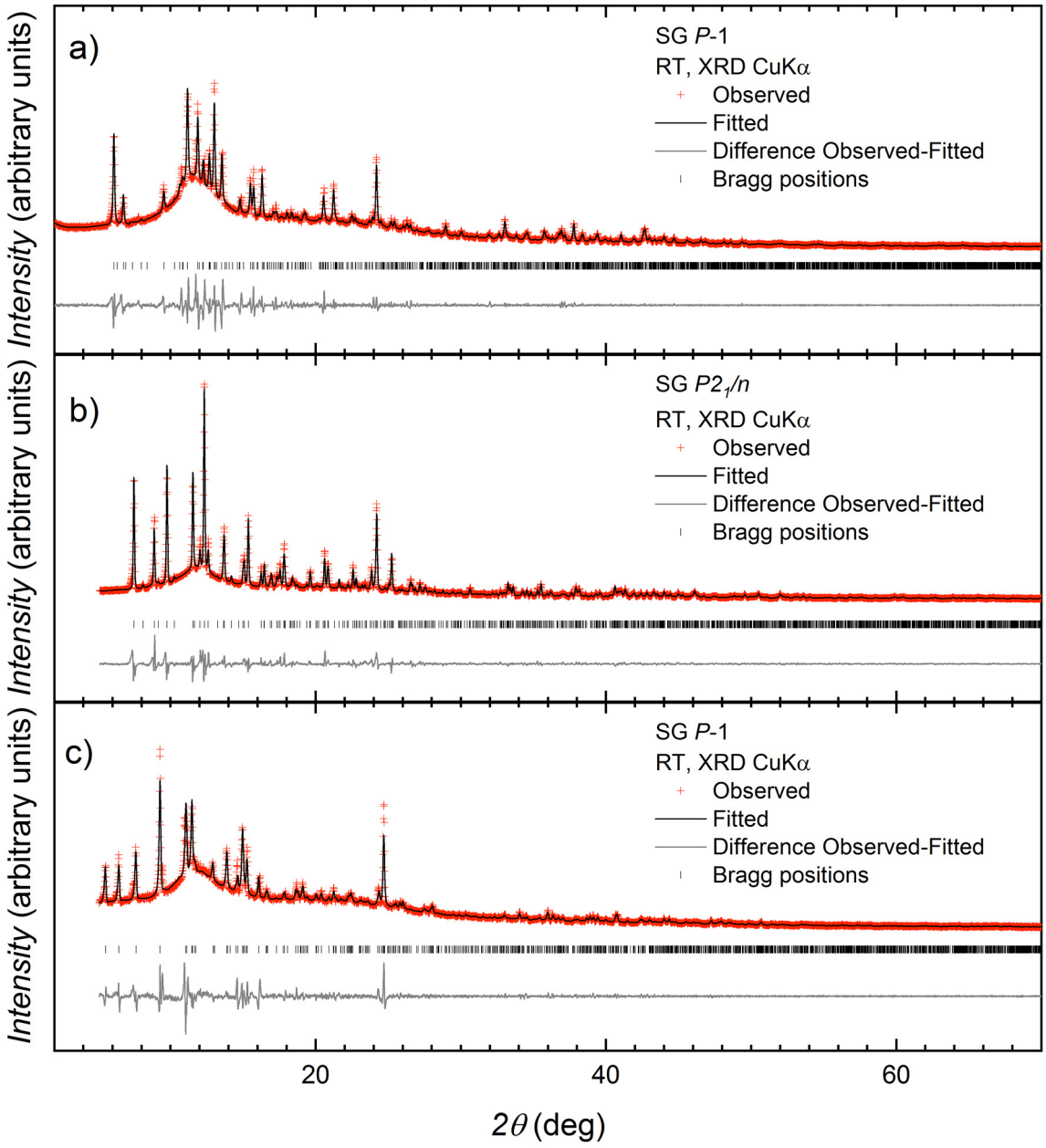

Figure 10. Laboratory X-ray diffraction (CuKα1 radiation) pattern (red crosses) of (**a**) [2{Cu_2(μ-OAc)$_4$(**2**)}·1.25MeOH]$_n$, (**b**) [Cu_2(μ-OAc)$_4$(**3**)]$_n$ and (c) [{Cu_2(μ-OAc)$_4$(**4**)}·0.2$CHCl_3$]$_n$ at room temperature. The black line corresponds to the best fit from the profile matching refinement. Lower vertical marks denote the Bragg peak positions. The bottom line in each plot represents the difference between experimental and calculated points.

The 1D coordination polymer chains in [2{Cu_2(μ-OAc)$_4$(**2**)}·1.25MeOH]$_n$, [{Cu_2(μ-OAc)$_4$(**4**)}·0.2$CHCl_3$]$_n$ and [Cu_2(μ-OAc)$_4$(**3**)]$_n$ are displayed in Figures 11–13, respectively. In each, the 3,2′:6′,3″-tpy domain exhibits conformation 2 (Scheme 2) in contrast to conformation 1 (Scheme 2) observed in [Cu_2(μ-OAc)$_4$(**1**)]$_n$. However, a comparison of Figures 11–13 reveals a further distinction between the coordination modes. In ligand-conformation 2, the outer nitrogen lone pairs point *in* or *out* with respect to the cavity defined by the central pyridine ring of the 3,2′:6′,3″-tpy unit (Scheme 6). If we consider the axial coordination sites of the paddle-wheel units in Figure 11 (working left to right across the diagram), we can define a coordination pattern along the chain as *out/in* for each {Cu_2(μ-OAc)$_4$} unit in [2{Cu_2(μ-OAc)$_4$(**2**)}·1.25MeOH]$_n$. Similarly, in Figure 12, the coordination

sequence is *out/in* for each $\{Cu_2(\mu\text{-}OAc)_4\}$ unit in $[Cu_2(\mu\text{-}OAc)_4(\mathbf{3})]_n$. However, in Figure 13, the chain in $[\{Cu_2(\mu\text{-}OAc)_4(\mathbf{4})\}\cdot 0.2CHCl_3]_n$ has the sequence *out/out* for one $\{Cu_2(\mu\text{-}OAc)_4\}$ unit followed by *in/in* for the next, and so on. The structure of the missing member of this series $[\{Cu_2(\mu\text{-}OAc)_4(\mathbf{5})\}\cdot 0.5MeOH]_n$ where **5** = 4′-(4-*n*-hexyloxyphenyl)-3,2′:6′,3″-tpy, has been reported by Zhang and coworkers [23]. As Figure S16 illustrates (see Supplementary Materials), the polymer chain possesses the same *in/in/out/out*... arrangement as we observe in the *n*-heptyloxy analogue $[\{Cu_2(\mu\text{-}OAc)_4(\mathbf{4})\}\cdot 0.2CHCl_3]_n$. The packing discussion that follows helps to rationalize the dependence of the coordination mode on the length of the alkyloxy tail.

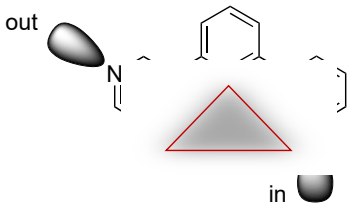

Scheme 6. With 3,2′:6′,3″-tpy in conformation 2 (defined in Scheme 2), the outer nitrogen lone pairs point in or out with respect to the cavity (red triangle) defined by the central pyridine ring.

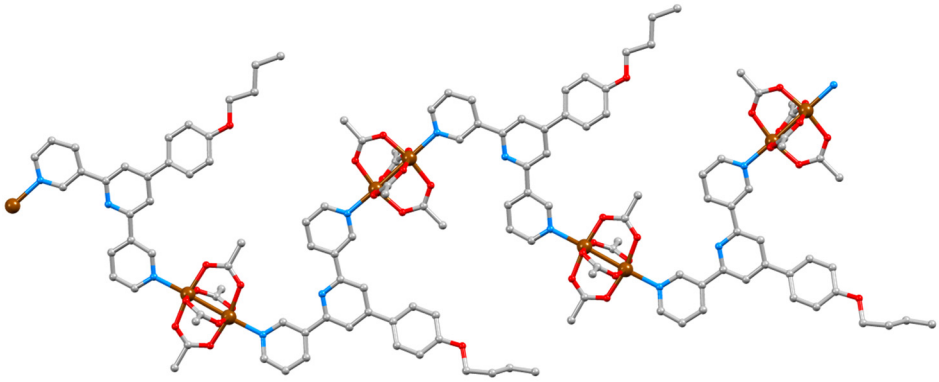

Figure 11. Part of one chain in $[2\{Cu_2(\mu\text{-}OAc)_4(\mathbf{2})\}\cdot 1.25MeOH]_n$ with a coordination sequence of *out/in* at each paddle-wheel unit; H atoms and solvent molecules omitted for clarity.

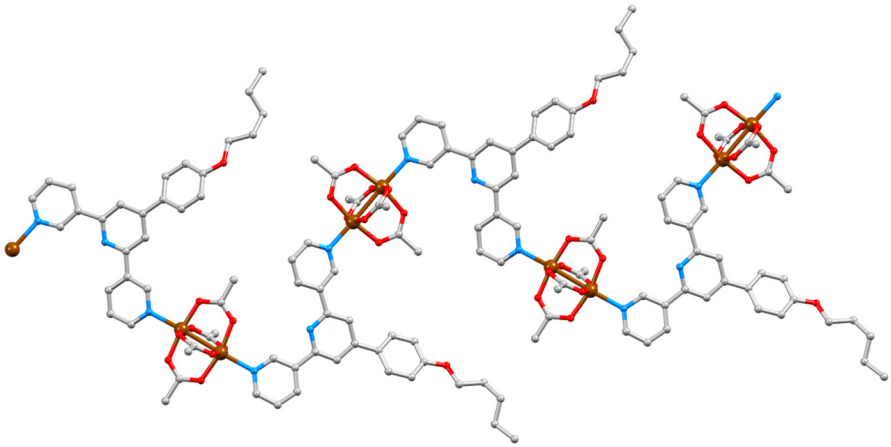

Figure 12. Part of one chain in $[Cu_2(\mu\text{-}OAc)_4(\mathbf{3})]_n$ with a coordination sequence of *out/in* at each paddle-wheel unit; H atoms are omitted.

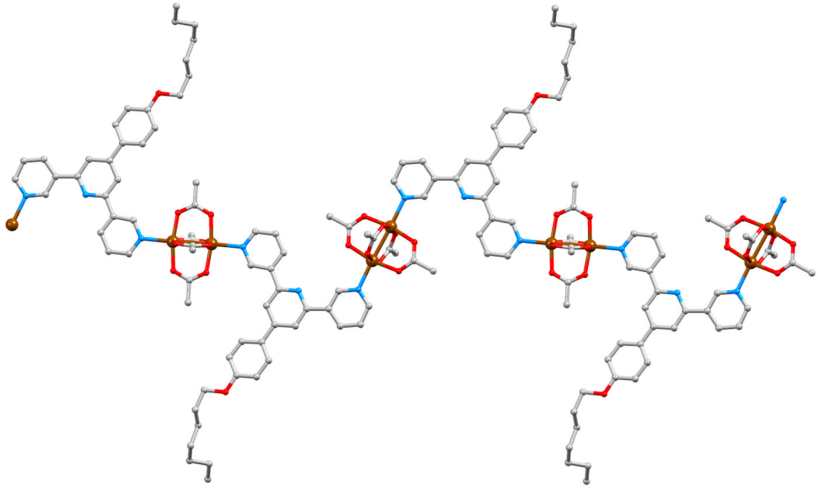

Figure 13. Part of one chain in $[\{Cu_2(\mu\text{-}OAc)_4(\mathbf{4})\}\cdot 0.2CHCl_3]_n$ with a coordination sequence of alternating *out/out* and *in/in* at each paddle-wheel unit. The *n*-heptyl chain is disordered. and only the major occupancy site is shown; H atoms and solvent molecules omitted for clarity.

In each of the three structures, the 1D coordination polymer chains pack side-by-side to form 2D sheets. Figure 14 compares the packing of two adjacent chains (each runs left to right in the figure as defined by the blue arrows) in $[2\{Cu_2(\mu\text{-}OAc)_4(\mathbf{2})\}\cdot 1.25MeOH]_n$ (Figure 14a), $[Cu_2(\mu\text{-}OAc)_4(\mathbf{3})]_n$ (Figure 14b) and $[\{Cu_2(\mu\text{-}OAc)_4(\mathbf{4})\}\cdot 0.2CHCl_3]_n$ (Figure 14c). At first glance, Figure 14a,b indicate similar packing, but closer inspection reveals a translational shift of chain 2 with respect to chain 1 on going from Figure 14a,b. While the *n*-butoxy chains are aligned to optimize van der Waals packing interactions (Figure 14a and Figure S17), pairs of *n*-pentyloxy chains are offset, and a potential interaction is partially interrupted by an acetato methyl group (Figure 14b). The space-filling representation in Figure 14b shows a centrosymmetric embrace between *n*-pentyloxy and methyl units. With an increase in the length of the alkyloxy tail to *n*-heptyloxy, the packing of polymer chains in a 2D sheet undergoes a significant change (Figure 14c) with van der Waals interactions between partly extended *n*-heptyloxy tails being the dominant in-sheet interactions. The cavity visible in Figure 14c is occupied, not by solvent molecules, but by ligands **4** from the next sheet.

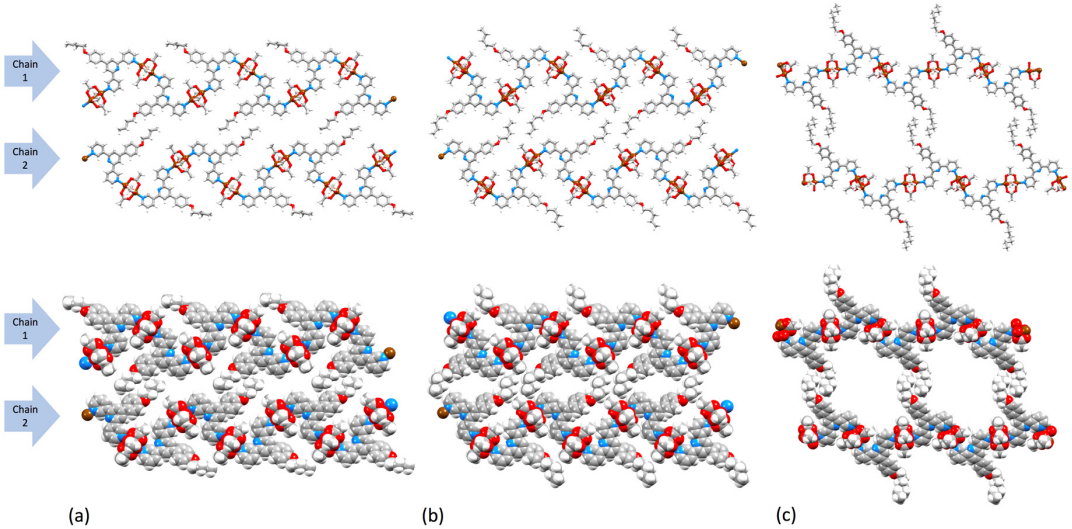

Figure 14. Packing of two adjacent chains (each runs left to right), shown in ball-and-stick and space-filling representations in (**a**) $[2\{Cu_2(\mu\text{-}OAc)_4(\mathbf{2})\}\cdot 1.25MeOH]_n$, (**b**) $[Cu_2(\mu\text{-}OAc)_4(\mathbf{3})]_n$, and (**c**) $[\{Cu_2(\mu\text{-}OAc)_4(\mathbf{4})\}\cdot 0.2CHCl_3]_n$. Solvent molecules in (**a**) and (**c**) are omitted. In (**c**), the *n*-heptyl chain is disordered, and only the major occupancy site is shown.

The differences in inter-sheet packing in $[2\{Cu_2(\mu\text{-}OAc)_4(\mathbf{2})\}\cdot 1.25MeOH]_n$, $[Cu_2(\mu\text{-}OAc)_4(\mathbf{3})]_n$ and $[\{Cu_2(\mu\text{-}OAc)_4(\mathbf{4})\}\cdot 0.2CHCl_3]_n$ are illustrated in Figure 15. In $[2\{Cu_2(\mu\text{-}OAc)_4(\mathbf{2})\}\cdot 1.25MeOH]_n$, each sheet comprising side-by-side packed 1D-polymer chains is essentially planar, and pairs of adjacent sheets interact through face-to-face π-stacking between centrosymmetric pairs of central pyridine rings of ligands **2** (inter-plane separation = 3.30 Å, centroid … centroid distance = 3.53 Å) (Figure 15a). The packing is similar in $[Cu_2(\mu\text{-}OAc)_4(\mathbf{3})]_n$ (Figure 15b) with an inter-plane separation between the π-stacked pyridine rings of 3.63 Å and a centroid … centroid separation of 4.33 Å. However, Figure 15b shows that the sheets in $[Cu_2(\mu\text{-}OAc)_4(\mathbf{3})]_n$ are ruffled in contrast to the planar sheets in $[2\{Cu_2(\mu\text{-}OAc)_4(\mathbf{2})\}\cdot 1.25MeOH]_n$. The packing undergoes a more significant change on going to $[\{Cu_2(\mu\text{-}OAc)_4(\mathbf{4})\}\cdot 0.2CHCl_3]_n$ (Figure 15c). Face-to-face interactions involve phenyl … pyridine … pyridine π-stacking.

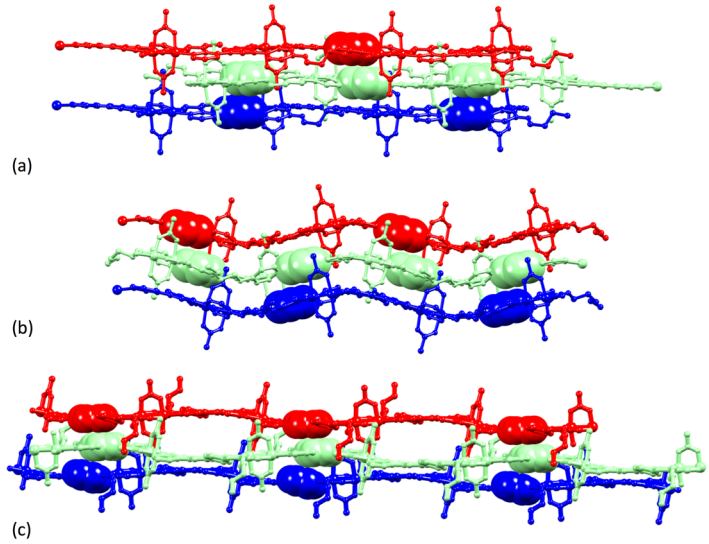

Figure 15. Packing of three adjacent 2D sheets (each comprising 1D polymer chains) in (**a**) $[2\{Cu_2(\mu\text{-}OAc)_4(\mathbf{2})\}\cdot 1.25MeOH]_n$, (**b**) $[Cu_2(\mu\text{-}OAc)_4(\mathbf{3})]_n$ and (**c**) $[\{Cu_2(\mu\text{-}OAc)_4(\mathbf{4})\}\cdot 0.2CHCl_3]_n$. Solvent molecules and H atoms are omitted.

4. Conclusions

We have investigated the reactions of the 4′-(4-alkyloxyphenyl)-3,2′:6′,3″-terpyridines **1**–**4** with $Cu(OAc)_2\cdot H_2O$. With a methoxy substituent (ligand **1**), we observe both the formation of $[Cu_2(\mu\text{-}OAc)_4(\mathbf{1})]_n$ (which contains the ubiquitous $\{Cu_2(\mu\text{-}OAc)_4\}$ paddle-wheel motifs) and $[\{Cu_4(\mu_3\text{-}OH)_2(\mu\text{-}OAc)_2(\mu_3\text{-}OAc)_2(AcO\text{-}\kappa O)_2(\mathbf{1})_2\}\cdot 2MeOH]_n$ in which centrosymmetric tetranuclear clusters link pairs of ligands **1** to give a double-stranded 1D-polymer. PXRD confirmed that a preparative scale reaction of **1** with $Cu(OAc)_2\cdot H_2O$ (1:2 molar ratio) immediately yields the blue microcrystalline 1D-coordination polymer $[Cu_2(\mu\text{-}OAc)_4(\mathbf{1})]_n$. However, crystal-growth conditions carried out by layering under ambient conditions in air over a period of several months yield predominantly the double-stranded 1D-coordination polymer $[\{Cu_4(\mu_3\text{-}OH)_2(\mu\text{-}OAc)_2(\mu_3\text{-}OAc)_2(AcO\text{-}\kappa O)_2(\mathbf{1})_2\}\cdot 2MeOH]_n$, with $[Cu_2(\mu\text{-}OAc)_4(\mathbf{1})]_n$ as a minor product. Crystal growth by layering a MeOH solution of $Cu(OAc)_2\cdot H_2O$ over a $CHCl_3$ solution of **2**, **3** or **4** produces blue crystals of $[2\{Cu_2(\mu\text{-}OAc)_4(\mathbf{2})\}\cdot 1.25MeOH]_n$, $[Cu_2(\mu\text{-}OAc)_4(\mathbf{3})]_n$ or $[\{Cu_2(\mu\text{-}OAc)_4(\mathbf{4})\}\cdot 0.2CHCl_3]_n$, all of which are single-stranded 1D coordination polymers.

In all five compounds, only the outer pyridine rings of the 3,2′:6′,3″-tpy unit coordinate to copper(II). However, in the polymers containing the $\{Cu_2(\mu\text{-}OAc)_4\}$ paddle-wheel units, the conformation of the 3,2′:6′,3″-tpy unit responds to changes in the length of the alkyloxy tails. In $[Cu_2(\mu\text{-}OAc)_4(\mathbf{1})]_n$, **1** adopts conformation 1 in Scheme 2, and a zigzag 1D chain results. In the polymers containing ligands **2**, **3** and **4**, the 3,2′:6′,3″-tpy adopts conformation 2 in Scheme 2, and van der Waals packing

forces between alkyloxy chains become important, complementing the π-stacking interactions between phenyl ... pyridine and pyridine ... pyridine rings.

Supplementary Materials: The following are available online at http://www.mdpi.com/2073-4360/12/2/318/s1. Figures S1 and S2: Mass spectra of **3** and **4**; Figures S3 and S4: Solid-state IR spectra of **3** and **4**; Figures S5–S8: HMQC and HMBC spectra of **3** and **4**; Figure S9: FTIR spectra; Figures S10 and S11: ORTEP diagrams of the asymmetric units in $[Cu_2(\mu\text{-}OAc)_4(\mathbf{1})]_n$ and $\{[Cu_4(\mu_3\text{-}OH)_2(\mu\text{-}OAc)_2(\mu_3\text{-}OAc)_2(AcO\text{-}\kappa O)_2(\mathbf{1})_2]\cdot 2MeOH\}_n$; Figure S12: Packing of chains in $\{[Cu_4(\mu_3\text{-}OH)_2(\mu\text{-}OAc)_2(\mu_3\text{-}OAc)_2(AcO\text{-}\kappa O)_2(\mathbf{1})_2]\cdot 2MeOH\}_n$; Figures S13–S15: ORTEP diagrams of the asymmetric units in $[2\{Cu_2(\mu\text{-}OAc)_4(\mathbf{2})\}\cdot 1.25MeOH]_n$, $[Cu_2(\mu\text{-}OAc)_4(\mathbf{3})]_n$ and $[Cu_2(\mu\text{-}OAc)_4(\mathbf{4})\}\cdot 0.2CHCl_3]_n$; Figure S16: Part of one chain in $[Cu_2(\mu\text{-}OAc)_4(\mathbf{5})\}\cdot 0.2CHCl_3]_n$; Figure S17: Packing of chains in $[2\{Cu_2(\mu\text{-}OAc)_4(\mathbf{2})\}\cdot 1.25MeOH]_n$.

Author Contributions: C.E.H. (Project conceptualization, administration, supervision, funding acquisition, manuscript writing); E.C.C. (Project conceptualization, administration, supervision, funding acquisition, manuscript editing); D.R. and G.M. (investigation, analysis, crystallography, manuscript writing); Y.M.K. and D.J.G. (powder diffraction, manuscript editing); A.P. (crystallography, manuscript editing). All authors have read and agreed to the published version of the manuscript.

Funding: This research was partially funded by the Swiss National Science Foundation (grant numbers 200020_182000 and 200020_182559).

Acknowledgments: We gratefully acknowledge the support of the University of Basel.

Conflicts of Interest: The authors declare no conflict of interest.

References

1. Chakrabarty, R.; Mukherjee, P.S.; Stang, P.J. Supramolecular Coordination: Self-Assembly of Finite Two- and Three-Dimensional Ensembles. *Chem. Rev.* **2011**, *111*, 6810–6918. [CrossRef]
2. Kalmutzki, M.J.; Hanikel, N.; Yaghi, O.M. Secondary building blocks as the turning point in the development of the reticular chemistry of MOFs. *Sci. Adv.* **2018**, *4*, eaat9180. [CrossRef] [PubMed]
3. Yaghi, O.M. Reticular Chemistry in All Dimensions. *ACS Cent. Sci.* **2019**, *5*, 1295–1300. [CrossRef] [PubMed]
4. Köberl, M.; Cokoja, M.; Herrmann, W.A.; Kühn, F.E. From molecules to materials: Molecular paddle-wheel synthons of macromolecules, cage compounds and metal–organic frameworks. *Dalton Trans.* **2011**, *40*, 6834–6859. [CrossRef] [PubMed]
5. Vagin, S.I.; Ott, A.K.; Rieger, B. Paddle-wheel zinc carboxylate clusters as building units for metal-organic frameworks. *Chem. Ing. Tech.* **2007**, *79*, 767–780. [CrossRef]
6. Handa, M.; Mikuriya, M.; Nukada, R.; Matsumoto, H.; Kasuga, K. Chain Compound of Molybdenum(II) Pivalate Bridged by 4,4′-Bipyridine. *Bull. Chem. Soc. Jpn.* **1994**, *67*, 3125–3127. [CrossRef]
7. Yao, Q.; Sun, J.; Li, K.; Su, J.; Peskov, M.V.; Zou, X. A series of isostructural mesoporous metal–organic frameworks obtained by ion-exchange induced single-crystal to single-crystal transformation. *Dalton Trans.* **2012**, *41*, 3953–3955. [CrossRef]
8. Chen, B.; Xiang, S.; Qian, G. Metal−Organic Frameworks with Functional Pores for Recognition of Small Molecules. *Acc. Chem. Res.* **2010**, *43*, 1115–1124. [CrossRef]
9. Li, B.; Wen, H.-M.; Cui, Y.; Zhou, W.; Qian, G.; Chen, B. Emerging Multifunctional Metal-Organic Framework Materials. *Adv. Mater.* **2016**, *28*, 8819–8860. [CrossRef]
10. Constable, E.C.; Housecroft, C.E. *Ligand and Metalloligand Design for Macrocycles, Multimetallic Arrays, Coordination Polymers and Assemblies*; Reedijk, J., Ed.; Elsevier: Amsterdam, The Netherlands. [CrossRef]
11. Constable, E.C.; Housecroft, C.E. Tetratopic bis(4,2′:6′,4″-terpyridine) and bis(3,2′:6′,3″-terpyridine) ligands as 4-connecting nodes in 2D-coordination networks and 3D-frameworks. *J. Inorg. Organomet. Polym. Mater.* **2018**, *28*, 414–427. [CrossRef]
12. Housecroft, C.E.; Constable, E.C. Ditopic and tetratopic 4,2′:6′,4″-Terpyridines as Structural Motifs in 2D- and 3D-Coordination Assemblies. *Chimia* **2019**, *73*, 462–467. [CrossRef]
13. Housecroft, C.E. 4,2′:6′,4″-Terpyridines: Diverging and Diverse Building Blocks in Coordination Polymers and Metallomacrocycles. *Dalton Trans.* **2014**, *43*, 6594–6604. [CrossRef] [PubMed]
14. Housecroft, C.E. Divergent 4,2′:6′,4″- and 3,2′:6′,3″-Terpyridines as Linkers in 2- and 3-Dimensional Architectures. *CrystEngComm* **2015**, *17*, 7461–7468. [CrossRef]

15. Dorofeeva, V.N.; Mishura, A.M.; Lytvynenko, A.S.; Grabovaya, N.V.; Kiskin, M.A.; Kolotilov, S.V.; Eremenko, I.L.; Novotortsev, V.M. Structure and Electrochemical Properties of Copper(II) Coordination Polymers with Ligands Containing Naphthyl and Anthracyl Fragments. *Theor. Exper. Chem.* **2016**, *52*, 111–118. [CrossRef]
16. Constable, E.C.; Housecroft, C.E.; Kopecky, P.; Neuburger, M.; Zampese, J.A.; Zhang, G. Coordination polymers with divergent 4′-tert-butyl-4,2′:6′,4″-terpyridine linkers: from aryl-aryl to ball-and-socket packing. *CrystEngComm.* **2012**, *14*, 446–452. [CrossRef]
17. Constable, E.C.; Housecroft, C.E.; Vujovic, S.; Zampese, J.A.; Crochet, A.; Batten, S.R. Do perfluoroarene ... arene and C–H...F interactions make a difference to 4,2′:6′,4″-terpyridine-based coordination polymers? *CrystEngComm* **2013**, *15*, 10068–10078. [CrossRef]
18. Zhang, G.; Jia, Y.-X.; Chen, W.; Lo, W.-F.; Brathwaite, N.; Golen, J.A.; Rheingold, A.L. Diverse zinc(II) coordination assemblies built on divergent 4,2′:6′,4″-terpyridine derivatives: syntheses, structures and catalytic properties. *RSC Adv.* **2015**, *5*, 15870–15879. [CrossRef]
19. Constable, E.C.; Housecroft, C.E.; Neuburger, M.; Schönle, J.; Vujovic, S.; Zampese, J.A. Molecular recognition between 4′-(4-biphenylyl)-4,2′:6′,4″-terpyridine domains in the assembly of d^9 and d^{10} metal ion-containing one-dimensional coordination polymers. *Polyhedron* **2013**, *60*, 120–129. [CrossRef]
20. Klein, Y.M.; Constable, E.C.; Housecroft, C.E.; Zampese, J.A.; Crochet, A. Greasy tails switch 1D-coordination $[Zn_2(OAc)_4(4'\text{-}(4\text{-}ROC_6H_4)\text{-}4,2':6',4''\text{-tpy})]_n$ polymers to discrete $[Zn_2(OAc)_4(4'\text{-}(4\text{-}ROC_6H_4)\text{-}4,2':6',4''\text{-tpy})_2]$ complexes. *CrystEngComm* **2014**, *16*, 9915–9929. [CrossRef]
21. Constable, E.C.; Zhang, G.; Coronado, E.; Housecroft, C.E.; Neuburger, M. Not just size and shape: spherically symmetrical d^5 and d^{10} metal ions give different coordination nets with 4,2′:6′,4″-terpyridines. *CrystEngComm* **2010**, *12*, 2139–2145. [CrossRef]
22. Song, J.; Wang, B.-C.; Hu, H.-M.; Gou, L.; Wu, Q.-R.; Yang, X.-L.; Shangguan, Y.-Q.; Dong, F.-X.; Xue, G.-L. In situ hydrothermal syntheses, crystal structures and luminescent properties of two novel zinc(II) coordination polymers based on tetrapyridyl ligand. *Inorg. Chim. Acta* **2011**, *366*, 134–140. [CrossRef]
23. Li, L.; Zhang, Y.Z.; Yang, C.; Liu, E.; Golen, J.A.; Zhang, G. One-dimensional copper(II) coordination polymers built on 4′-substituted 4,2′:6′,4″- and 3,2′:6′,3″-terpyridines: Syntheses, structures and catalytic properties. *Polyhedron* **2016**, *105*, 115–122. [CrossRef]
24. Tian, Y.; Xiao, L. CSD Communication, refcode CACXEM, 2015. [CrossRef]
25. Xiao, L.; Tian, Y. CSD Communication, refcode VUKMOF, 2015. [CrossRef]
26. Constable, E.C.; Housecroft, C.E.; Neuburger, M.; Vujovic, S.; Zampese, J.A.; Zhang, G. Cobalt(II) coordination polymers with 4′-substituted 4,2′:6′,4″- and 3,2′:6′,3″-terpyridines: engineering a switch from planar to undulating chains and sheet. *CrystEngComm.* **2012**, *14*, 3554–3563. [CrossRef]
27. Lu, L.; Wang, J.; Wu, W.-P.; Ma, A.; Liu, J.-Q.; Yadav, R.; Kumar, A. Fluorescent sensing of nitroaromatics by two coordination polymers having potential active sites. *J. Luminescence* **2017**, *186*, 40–47. [CrossRef]
28. Klein, Y.M.; Prescimone, A.; Constable, E.C.; Housecroft, C.E. Coordination behaviour of 1-(4,2′:6′,4″-terpyridin-4′-yl)ferrocene and 1-(3,2′:6′,3″-terpyridin-4′-yl)ferrocene: predictable and unpredictable assembly algorithms. *Aust. J. Chem.* **2017**, *70*, 468–477. [CrossRef]
29. Wang, T.-T.; Zhang, J.-L.; Hu, H.-M.; Cheng, Y.; Xue, L.-L.; Wang, X.; Wang, B. Syntheses, structures and luminescent properties of Zn/Cd coordination polymers based on 4′-(2-carboxyphenyl)-3,2′:6′,3″- terpyridine. *Polyhedron* **2018**, *151*, 43–50. [CrossRef]
30. Zhang, L.; Li, C.-J.; He, J.-E.; Chen, Y.-Y.; Zheng, S.-R.; Fan, J.; Zhang, W.-G. Construction of New Coordination Polymers from 4′-(2,4-disulfophenyl)-3,2′:6′3″-terpyridine: Polymorphism, pH-dependent syntheses, structures, and properties. *J. Solid State Chem.* **2016**, *233*, 444–454. [CrossRef]
31. Yang, P.; Wang, M.-S.; Shen, J.-J.; Li, M.-X.; Wang, Z.-X.; Shao, M.; He, X. Seven novel coordination polymers constructed by rigid 4-(4-carboxyphenyl)-terpyridine ligands: Synthesis, structural diversity, luminescence and magnetic properties. *Dalton Trans.* **2014**, *43*, 1460–1470. [CrossRef]
32. Yoshida, J.; Nishikiori, S.; Yuge, H. Bis(3-cyano-pentane-2,4-dionato) Co(II) as a linear building block for coordination polymers: combinations with two polypyridines. *J. Coord. Chem.* **2013**, *66*, 2191–2200. [CrossRef]

33. Rocco, D.; Prescimone, A.; Klein, Y.M.; Gawryluk, D.J.; Constable, E.C.; Housecroft, C.E. Competition in coordination assemblies: 1D-coordination polymer or 2D-nets based on $Co(NCS)_2$ and 4′-(4-methoxyphenyl)-3,2′:6′,3″-terpyridine. *Polymers* **2019**, *11*, 1224. [CrossRef]
34. Rocco, D.; Housecroft, C.E.; Constable, E.C. Synthesis of Terpyridines: Simple Reactions – What Could Possibly Go Wrong? *Molecules* **2019**, *24*, 1799. [CrossRef]
35. Software for the Integration of CCD Detector System Bruker Analytical X-ray Systems. Bruker axs: Madison, WI, USA, (after 2013).
36. Sheldrick, G.M. ShelXT-Integrated space-group and crystal-structure determination. *Acta Cryst.* **2015**, *A71*, 3–8. [CrossRef]
37. Dolomanov, O.V.; Bourhis, L.J.; Gildea, R.J.; Howard, J.A.K.; Puschmann, H. Olex2: A Complete Structure Solution, Refinement and Analysis Program. *J. Appl. Cryst.* **2009**, *42*, 339–341. [CrossRef]
38. Sheldrick, G.M. Crystal Structure Refinement with ShelXL. *Acta Cryst.* **2015**, *C27*, 3–8. [CrossRef]
39. Palatinus, L.; Chapuis, G. Superflip—A Computer Program for the Solution of Crystal Structures by Charge Flipping in Arbitrary Dimensions. *J. Appl. Cryst.* **2007**, *40*, 786–790. [CrossRef]
40. Palatinus, L.; Prathapa, S.J.; van Smaalen, S. EDMA: A Computer Program for Topological Analysis of Discrete Electron Densities. *J. Appl. Cryst.* **2012**, *45*, 575–580. [CrossRef]
41. Macrae, C.F.; Edgington, P.R.; McCabe, P.; Pidcock, E.; Shields, G.P.; Taylor, R.; Towler, M.; van de Streek, J. Mercury: Visualization and Analysis of Crystal Structures. *J. Appl. Cryst.* **2006**, *39*, 453–457. [CrossRef]
42. Macrae, C.F.; Bruno, I.J.; Chisholm, J.A.; Edgington, P.R.; McCabe, P.; Pidcock, E.; Rodriguez-Monge, L.; Taylor, R.; van de Streek, J.; Wood, P.A. Mercury CSD 2.0—New Features for the Visualization and Investigation of Crystal Structures. *J. Appl. Cryst.* **2008**, *41*, 466–470. [CrossRef]
43. Rietveld, H.M. A Profile Refinement Method for Nuclear and Magnetic Structures. *J. Appl. Cryst.* **1969**, *2*, 65–71. [CrossRef]
44. LeBail, A.; Duroy, H.; Fourquet, J.L. Ab-initio structure determination of $LiSbWO_6$ by X-ray powder diffraction. *Mat. Res. Bull.* **1988**, *23*, 447–452. [CrossRef]
45. Pawley, G.S. Unit-cell refinement from powder diffraction scans. *J. Appl. Cryst.* **1981**, *14*, 357–361. [CrossRef]
46. Rodríguez-Carvajal, J. Recent Advances in Magnetic Structure Determination by Neutron Powder Diffraction. *Phys. B* **1993**, *192*, 55–69. [CrossRef]
47. Roisnel, T.; Rodríguez-Carvajal, J. WinPLOTR: A Windows tool for powder diffraction patterns analysis Materials Science Forum. In Proceedings of the Seventh European Powder Diffraction Conference (EPDIC 7), Barcelona, Spain, 20–23 May 2000; pp. 118–123.
48. Wang, J.; Hanan, G.S. A Facile Route to Sterically Hindered and Non-hindered 4′-Aryl-2,2′:6′,2″- terpyridines. *Synlett* **2005**, 1251–1254. [CrossRef]
49. Alsalme, A.; Ghazzali, M.; Khan, R.A.; Al-Farhan, K.; Reedijk, J. A novel trinuclear μ_3-hydroxido-bridged Cu(II) compound; a molecular cluster, stabilized by hydrogen bonding, bridging pyrazolates, terminal pyrazoles, water and nitrate anions. *Polyhedron* **2014**, *72*, 64–67. [CrossRef]
50. Bette, S.; Kremer, R.K.; Eggert, G.; Tang, C.C.; Dinnebier, R.E. On verdigris, part I: synthesis, crystal structure solution and characterisation of the 1–2–0 phase ($Cu_3(CH_3COO)_2OH)_4$). *Dalton Trans.* **2017**, *46*, 14847–14858. [CrossRef]
51. Ferraro, J.R.; Walker, W.R. Infrared Spectra of Hydroxy-Bridged Copper(II) Compounds. *Inorg. Chem.* **1965**, *4*, 1382–1386. [CrossRef]
52. Janiak, C. A critical account on π–π stacking in metal complexes with aromatic nitrogen-containing ligands. *J. Chem. Soc. Dalton Trans.* **2000**, 3885–3896. [CrossRef]
53. Groom, C.R.; Bruno, I.J.; Lightfoot, M.P.; Ward, S.C. The Cambridge Structural Database. *Acta Crystallogr.* **2016**, *B72*, 171–179. [CrossRef]
54. Lah, N.; Koller, J.; Giester, G.; Segedin, P.; Leban, I. Copper(II) carboxylates with 4-aminopyridine: neutral mononuclear structures, isomerism of aceto compounds and a novel tetranuclear structure. *New J. Chem.* **2002**, *26*, 933–938. [CrossRef]
55. Mezei, G.; Rivera-Carrillo, M.; Raptis, R.G. Effect of copper-substitution on the structure and nuclearity of Cu(II)-pyrazolates: from trinuclear to tetra-, hexa- and polynuclear complexes. *Inorg. Chim. Acta* **2004**, *357*, 3721–3732. [CrossRef]

56. de Campos, N.R.; Ribeiro, M.A.; Oliveira, W.X.C.; Reis, D.O.; Stumpf, H.O.; Doriguetto, A.C.; Machado, F.C.; Pinheiro, C.B.; Lloret, F.; Julve, M.; et al. Magneto-structural versitility of copper(II)-3-phenylpropionate coordination polymers with N-donor coligands. *Dalton Trans.* **2016**, *45*, 172–189. [CrossRef]
57. Zhou, J.-H.; Cheng, R.-M.; Song, Y.; Li, Y.-Z.; Yu, Z.; Chen, X.-T.; Xue, Z.-L.; You, X.-Z. Syntheses, Structures, and Magnetic Properties of Unusual Nonlinear Polynuclear Copper(II) Complexes Containing Derivatives of 1,2,4-Triazole and Pivalate Ligands. *Inorg. Chem.* **2005**, *44*, 8011–8022. [CrossRef]